MESOSCALE VARIABILITY IN THE BLACK SEA; SATELLITE OBSERVATIONS AND LABORATORY EXPERIMENTS

MARINA BLOKHINA

Mesoscale variability in the Black Sea:
satellite observations and laboratory experiments

by

Marina Blokhina

A thesis submitted to the
School of Graduate Studies
in partial fulfillment of the
requirements for the degree of
Master of Science

Department of Physics and Physical Oceanography
Memorial University of Newfoundland

December 2003

St. John's Newfoundland

Your file Votre référence
ISBN: 0-612-99053-2
Our file Notre référence
ISBN: 0-612-99053-2

Abstract

The circulation in the Black Sea is characterized by a strong basin-wide current along the shore in the cyclonic direction known as the Rim Current. Satellite and field data demonstrate that this circulation is subject to mesoscale variability in the form of meanders, intense jets, eddies and filaments. In this thesis the surface circulation of the Black Sea is simulated in the laboratory experiments and analyzed using the satellite data. This work focuses on improvement of methods for analyzing the satellite images in order to investigate the Black Sea mesoscale dynamics and to understand the physics of eddies, air-sea interaction and circulation. In this work we develop a new approach to the measurement of velocity and vorticity fields of the upper layer of the Black Sea, using direct observations made by National Oceanic and Atmospheric Administration (NOAA) Advanced Very-High Resolution Radiometer (AVHRR) during 2000-2002 years. The analysis is based on the Maximum Cross Correlation (MCC) analysis and Particle Image Velocimetry (PIV) method. The application of these two techniques to the Black Sea investigation reveals the large scale dynamic feature of circulation, as well as many details of mesoscale vortical activity. The results demonstrate the main characteristics of the Black Sea circulation. In particular, the Black Sea Rim Current is well defined by an average velocity of 20 cm/s. The Rim Current intensifies along the Turkish coast and displays a meandering structure with essential seasonal variability.

The unstable cyclonic boundary current was modeled in a new series of laboratory experiments on a rotating platform using a scaled model of the Black Sea. The dynamical similarity of the important dimensionless control parameters, including the normalized Rossby deformation radius, the Rossby number and the Ekman number, was satisfied in the experiments. The results demonstrate the development of baroclinic instability due to fresh water discharge imitating the river inflow in the Black Sea. Persistent transient features of the circulation, such as the so-called Batumi Eddy and the Sevastopol Eddy as well as other features, were reproduced in the experiments when the background rotation rate of the system was varied.

Acknowledgements

This thesis would not exist at all without Dr. Yakov Afanasyev, who has believed in my project, has supported me strongly through all this work, and has indulged my inquisitiveness even more often than I had hoped.

I would particularly like to thank Gleb Panteleev for our friendship, sharing his knowledge and for kindly and patiently helping me with so many details in Fortran and the variational method.

I should also mention my examiners Professors Brad de Young and Daniel Bourgault. Their competent and meticulous reviews of this thesis, and their astute comments and questions were invaluable.

Special and inexpressible gratitude to my family for endless concern, love, support and preventing me from going crazy.

Grateful acknowledgment goes to Nick Record for proofreading all this work and not falling asleep after the first pages.

In addition, it was marvelous to meet so many new people and to see new places. Many thanks to my colleagues and friends for all the fun and collaboration

These are only a few names, since I cannot adequately acknowledge all of the people to whom I am indebted. I hope the rest will know that I thank them very much.

I thank all people who have already read and who will ever read this manuscript for their at least virtual interest and not getting bored after the reading.

TABLE OF CONTENTS

List of Tables

List of Figures

CHAPTER 1.

Introduction

1.1.Location

The Black Sea (Figure 1) is a nearly enclosed basin, having limited exchange with the Mediterranean through the narrow Bosphorus Strait. The net outflow from the Black Sea through the Bosphorus Strait is approximately 300 km^3/yr [Unluata et al. (1990)] which constitutes 0.06% of the total volume of the Black Sea. The sea is elongated in the east-west direction with an aspect ratio of approximately 3:1. The Black Sea is relatively narrow in its central part between the Crimean peninsula and the Anatolian coast where the shortest distance is 260 km. The limited latitudinal extent of the sea allows us to exclude the effect of the variation of the Coriolis parameter with latitude from consideration of the dynamical features of the circulation.

The seafloor is divided into the shelf, the continental slope and the deep-sea depression. The shelf, or continental shoal, is the direct continuation of dry land covered by the sea. It now occupies a large area in the northwestern part of the Black Sea, where the shelf is over 200 km wide with a typical depth ranging from 0 to 100 m, and reaching up to 160 m in some places. In other parts of the sea, it has a depth of less than 100 m and a width of 2.2 to 15 km. Near the Caucasian and Anatolian coasts the shelf is only a narrow intermittent strip. The shelf transitions to a rather steep continental slope, descending at an average angle of 5-8° in the north-western part and 1-3° near the Kerch Strait . In some sections the gradient reaches 20-30°.

The underwater extensions of the Danube, the Dniester, and the Dnieper river valleys are on the north-western shelf, a long distance out to sea, approximately 100-120 km from the coast.

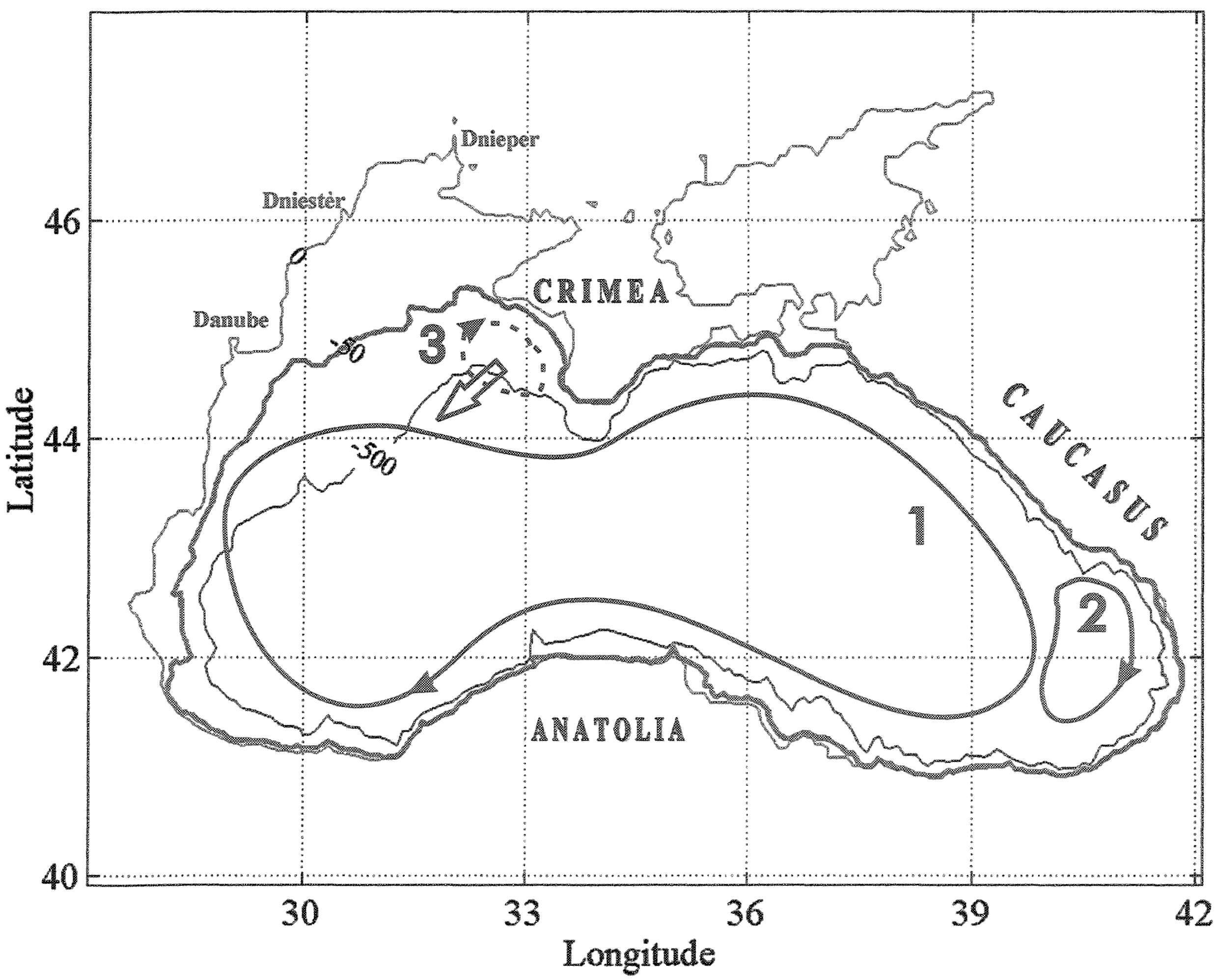

Figure 1. Bathymetry and the sketch of the main features of the circulation of the Black Sea: Rim Current (1); Batumi Eddy (2); Sevastopol Eddy (3). The arrow indicates the general direction of the migration of the Sevastopol Eddy

1.2. Circulation characteristics.

The hydrological structure of the Black Sea is characterized by a very stable stratification. The surface salinity fluctuates around 18 psu, while the bottom salinity can reach up to 22-23 psu. The main reason for the low salinity of the Black Sea is the positive water balance of the sea and the limited exchange with the Mediterranean. The general water exchange model for the sea according to Falkner et al. (1991) is presented in Figure 2. The river input and precipitation far exceed the evaporation. Since the input of waters exceeds evaporation, there is a net flux through the Bosphorus going into the Marmara Sea and from there to the Mediterranean. Most of the fresh water inflow comes in to the western part of the sea from four major rivers: the Danube, the Dniester, the Dnieper and the Southern Bug. According to the Technical Report (2002) of European Environment Agency, the average total annual discharge into the north-west of the sea for the period 1921 -1988 was 261 km^3 per year, which constitutes approximately 0.05% of the total volume of the Black Sea. The net fresh water input however has substantial seasonal and interannual variability. The Danube is the largest contributor, accounting for more than 50% of the total runoff [Ozsoy & Unluata (1997)]. The stratification is especially pronounced along the coast in the boundary current [e.g. Oguz & Besiktepe (1999)] called the Rim Current [Oguz et al. (1992)], transporting fresh water around the sea in a cyclonic direction. This basin scale current is also referred to as the Main Black Sea Current in Russian literature [e.g. Filippov (1968), Titov (2002), Eremeev, (1992), and references therein].

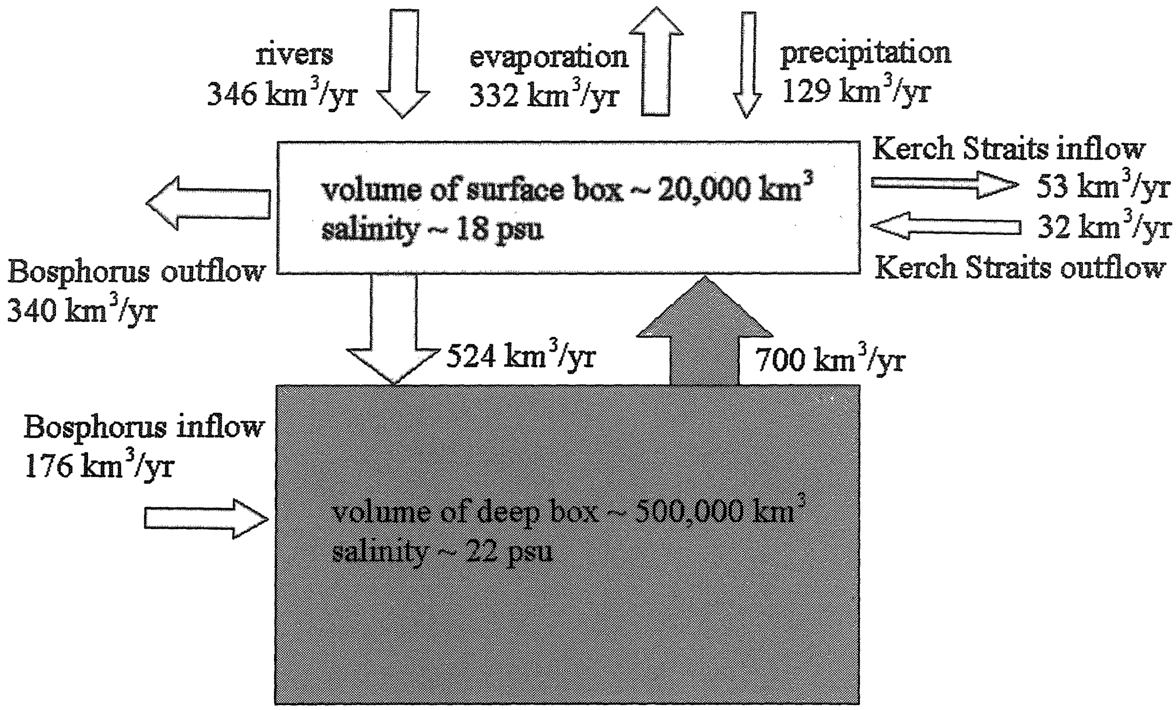

Figure 2. The water exchange model for the Black Sea, including its two main water masses. The graph is reproduced with some changes from Falkner et al. (1991)

Salinity stratification limits vertical convection, creating the permanent halocline and pycnocline. Their typical depth is 100-200 m. Such a two-layer stratified system allows one to use a straightforward approach to modeling the hydrological structure of the Black Sea in the laboratory.

The general circulation of the Black Sea is characterized by a basin scale cyclonic boundary current [e.g. Newmann (1942); Bogatko et al. (1979)]. This coastal current exhibits frequent episodes of instability, culminating in filaments and eddies. Coastal currents along the southern continental margin of the Black Sea undergo marked seasonal variations associated with seasonal change in the prevailing winds and river discharge. Two interconnected large-scale cyclonic gyres are formed in the interior of the western and eastern parts of the basin due to the narrowing in the central part of the sea. Persistent or recurrent features of this basin-wide circulation are also anticyclonic eddies along the coast. Some “taxonomy” of these features of the surface circulation of the Black Sea is provided in Oguz et al. (1993) and with some revisions in Korotaev et al. (2003). Some features are particularly worth noting in the context of the numerical and experimental results reported herein. One large anticyclonic eddy occupying the southeastern corner of the Black Sea is called the Batumi Eddy. It is formed by the recirculation to the right of the Rim Current. The current separates from the coast in this region and crosses the sea towards the northern shore at approximately 40^{o} E. Another persistent anticyclonic eddy (Sevastopol Eddy) is located on the west of the tip of the Crimean peninsula. It is similarly located to the right of the main jet of the Rim current which separates from the coast following the continental slope in this region. According to Ginzburg et al. (2002 b), the Sevastopol Eddy often migrates slowly in the southwest direction (arrow in Figure 1). Both of these eddies exhibit significant variability during the year. It can be clearly seen in the geostrophic velocity maps deduced from the TOPEX/Poseidon altimeter data [see Figure 9 in Korotaev et al. (2001)] that the Batumi Eddy starts to appear in winter and is strongest in spring while in summer and fall it is undistinguishable. Moreover, in summer and fall the separation of the jet from the northern shore rather than from the southern shore can be observed. This can result in a reversal of the circulation in the region of the Batumi Eddy although the reversed circulation is weaker than the circulation associated with the Batumi Eddy. The origin of the Batumi Eddy is still a subject of debate, and its existence is sometimes attributed to the surface freshwater forcing associated with the intensification of precipitation toward the eastern coast of the Black Sea.

Herein we will argue that the Batumi Eddy is a transient feature of the circulation, occurring as a result of the separation of the boundary current due to variations of the intensity of the general circulation. The Sevastopol Eddy is subject to even stronger variability. In fact, the identity of this eddy is artificial to large extent. Satellite imagery of this region of the sea often reveals two smaller anticyclones or even anticyclones accompanied by cyclonic eddies [Ginzburg et al. (2000)]. This combination constitutes a vortex dipole or mushroom-like current. Numerous recent observations [e.g. Fedorov and Ginzburg (1992) Ginzburg, (1994, 1995), Ginzburg et al. (2000), Afanasyev et al. (2002), Ginzburg et al. (2002 a, b)] using the satellite imagery demonstrate significant mesoscale variability of the entire circulation system. The observed mesoscale features of the circulation include meanders, closely spaced anticyclonic and cyclonic eddies, dipoles and filaments. These hydrodynamical structures are also typical features of any quasi-two-dimensional turbulent flow [e.g. Voropayev, Afanasyev, (1994)]. It is especially worth noting that regular arrays of meanders are often observed along the southern coast between 30^{o} E and 40^{o} E [e.g. Figure 8 in Oguz & Besiktepe (1999); Figure 1 in Ginzburg et al. (2000) and Figure 5 in Afanasyev et al. (2002)]. These meanders are likely due to the baroclinic instability of the Rim Current modified by the coastal features in this region. Similar instability is also observed on the northern shore of the Black Sea. The temporal and spatial characteristics of the mesoscale variability in the Black Sea as well as dynamical processes involved are yet to be fully understood. It is important to study these flows not only because of their many practical connections such as the understanding of exchange between the shelf region and the interior of the sea, but also because such flows often reveal the influence of fundamental hydrodynamic interactions.

The major mechanisms that force cyclonic circulation in the Black Sea are the buoyancy flux due to river input and the wind stress. The importance of the relative contributions of these two mechanisms is not completely clear. The buoyancy flux alone can provide the required cyclonic circulation according to the theoretical and experimental analysis of Bulgakov et al. (1996 a, b). Recent estimates [Efimov & Shokurov (2002), Efimov et al. (2002)], however, show that the seasonal variability of the circulation system is correlated with the vorticity of wind over the sea. The spatial extent of wind fields is larger than that of the Black Sea. The annual cycle of wind vorticity follows a simple harmonic law such that the cyclonic vorticity prevails in winter while the anticyclonic vorticity is persistent in summer. The amplitudes of the cyclonic and anticyclonic peaks are slightly different with a positively signed (cyclonic) annual average value of 10^{-6} s^{-1}, which constitutes approximately 25 - 35% of the peak values. It is also worth noting that river discharge also follows an annual cycle with the maximum value occurring in May and the minimum in October. The seasonal variability of the discharge is significant. The difference between the peak and the mean value constitutes approximately 75% of the mean [Kourafalou & Stanev (2001)]. The overall intensity of the circulation in the Black Sea also exhibits a strong seasonal variation. It attenuates in summer to fall and intensifies in winter to spring [Korotaev et al. (2001)]. The Rim Current jet is clearly observed in winter and spring, while during summer months the mesoscale eddy variability is so large that it masks the Rim Current such that it can only be defined in terms of statistically defined transport. The temporal evolution of kinetic energy of the surface geostrophic circulation derived from the TOPEX/Poseidon altimeter data [see Figure 10 in Korotaev et al. (2001)] is characterized by a strong peak in January and February which can be associated with atmospheric forcing and a weaker peak in May which is probably due to the intensified river discharge. The variability of the kinetic energy can be as high as 70% of the mean value.

In recent years, numerous attempts have been made to model different dynamical aspects of the circulation of the Black Sea in numerical simulations [e.g. Oguz & Malanotte-Rizzoli, (1996), Demyshev et al. (1996), Stanev & Beckers (1999), Staneva et al. (2001), Stanev & Staneva (2000), Knysh et al. (2001), Maderich & Konstantinov (2002), Beckers et al. (2002)]. However, numerical simulations are subject to difficulties in combining all available data and forcing with simplified models in a simplified basin. The numerical results still do not give a realistic output for long periods. The importance of forcing on the seasonal dynamics is considered in the numerical simulations of Maderich & Konstantinov (2002). Their one-and-a-half dimensional model of stratified sea describes seasonal variations of the vertical structure. The model is forced by using time series of the wind, air temperature and freshwater influx. Nevertheless, comparison of observations on an annual scale with simulations gives very poor results. Stanev & Staneva (2000) analyzed the influence of baroclinic eddies on the changes of the Black Sea circulation. They demonstrated that baroclinic instability might lead to interannual changes. Two possible regimes of surface circulation were considered: first, when basin circulation with a large gyre encompassing the whole basin is dominant, and the second, when the gyre disintegrates into many small eddies. However, the model variability was not regular and transition between two regimes was rather arbitrary and did not follow the forcing variability. The obtained results were also utterly sensitive to model resolution.

A great amount of information about the dynamics of the sea surface can be obtained by analyzing satellite images. Such observations are characterized by high space and time resolution. The uniformity of the images and their regularity enable them to be a unique source for investigating the surface circulation. The analysis of remotely sensed information is at present a powerful tool of oceanographic studies in all regions of the World Ocean. The data collected by satellites since the late 1970's provide oceanographers with a large volume of information on the state of the ocean surface although these data are not always accurate enough. The remotely sensed information is available to scientists either directly from the satellites, being received by the local stations and processed directly by users, or disseminated via Internet after processing at large centers. The most important remote sensing instruments are infrared sensors collecting data on Sea Surface Temperature (*SST*), altimeters obtaining anomalies of Sea Surface Height (*SSH*), and the sensors working within the visible light band. The most popular and numerous studies are those where altimetric data accumulated by the Topex/ Poseidon satellite are used [e. g. Korotaev & Khomenko (2003), Stanev et al. (2000), Korotaev et al. (2001) and references therein]. However, proper use of altimetric observations requires a variety of corrections crucially reducing the accuracy, and only geostrophic currents and their large-scale components can be considered in such research. Using an approach proposed in this thesis, instantaneous velocity fields and vorticity distribution can be obtained.

Satellite data (visible, IR, and sea color) with a spatial resolution of ~1 km and a temporal resolution of a few hours (up to six images per day) are necessary for studies of dynamics of mesoscale and small-scale structures. Daily satellite monitoring of the Black Sea, which has been performed since 1994 by the Remote Sensing Department of the Marine Hydrophysical Institute (MHI) in Sevastopol (Ukraine), have already produced interesting results on specific features of local circulation in the northwestern, southeastern, and northeastern Black Sea in summer and autumn [Ginzburg et al. (1994, 1995, 1998, 2000, 2002a, 2002b)].

There are relatively few laboratory experiments on this subject. Bulgakov et al. (1996 b) considered the process of development of quasi-stationary circulation induced by buoyancy fluxes in a rotating basin. It was demonstrated that the slow injection of fresh water at the surface and saltier water at an intermediate depth results in the formation of a cyclonic circulation at the surface with a countercurrent at an intermediate depth. A similarity of a number of control parameters including the Rossby and Ekman numbers was achieved in the experiments. The formation of the stationary circulation was observed on a significant time scale of several hours which was mainly controlled by the time scale of viscosity. The addition of a simple coastline in the form of two convex plates in the circular tank allowed the authors to show the formation of two macro gyres. The issue of variability of the general cyclonic circulation was considered in laboratory experiments by Zatsepin et al. (2002). The cyclonic circulation in a circular tank was forced by a freshwater source at the surface. It was observed that the flow was stable initially when the value of the Burger number, which was defined as the baroclinic Rossby deformation radius normalized by the characteristic size of the basin, was high enough. After some significant time, the upper layer was formed over the entire surface area, and the value of the Burger number became lower. The flow began meandering, eventually filling with eddies the entire area of the basin. The different parameters for the Black Sea and those that were used in laboratory experiments of Bulgakov et al. (1996) and Zatsepin et al. (2002) are given in the Table 1.

Table 1. Comparative parameters using in different laboratory experiments and those of the Black Sea.

Parameter	The Black Sea	Experiments of Bulgakov et al. (1996)	Experiments of Zatsepin et al. (2002)
Fresh water discharge, Q, cm^3/s	6×10^9	1	0.5-9
$\delta\rho/\rho_0$	10^{-2}	10^{-3}	-
Coriolis parameter, f, s^{-1}	10^{-4}	0.3	5.4
The salinity increment between the upper and lower layers, ΔS, $^0/_{00}$	3	1.4 - 2.8	20 - 28
Coefficient of the saline compression, β, $(^0/_{00})^{-1}$	8×10^{-4}	8×10^{-4}	7×10^{-4}
Coefficient of viscosity, ν, cm^2/s	1	10^{-2}	10^{-2}
Horizontal scale, L, cm	4×10^7-6×10^7	20	40
Total depth, H, cm	2×10^5	10	15
Upper layer, h, cm	1.5-2×10^4	2	≤ 2
Rossby deformation radius R_d, cm	1.5-2.5×10^6	7	1- 2
The ratio R/L	0.03	0.35	0.05
Rossby number, Ro	0.01 - 0.02	0.25	-
The horizontal flow velocity, U, cm/s	~ 40	0.4	-
The Burger number, Bu	0.006 - 0.02	0.12	0.0025
The Froude number, Fr	0.05 - 0.5	0.28	-
The Ekman number, Ek	10^{-6} - 10^{-4}	3×10^{-4}	$\sim 10^{-3}$

1.3. Baroclinic Instability (Theoretical Background).

Instability processes in the ocean are traditionally divided into barotropic and baroclinic instability. Barotropic instability is the process where mesoscale features (meanders, filaments, eddies) develop from a basic state by conversion of kinetic energy from the basic state to the eddy field [Rayleigh (1880), Kuo (1949), Fjørtoft (1950)]. In contrast, baroclinic instability is the process in which the energy source for disturbance growth is available potential energy [Eady (1949), Phillips, (1951)].

Baroclinic instability is of central importance to eddy production in midlatitude oceans and atmospheres at the scale of the Rossby radius of deformation [de Verdiere & Huck (1999)]. The mechanism of baroclinic instability gives a method whereby a small perturbation of the basic steady flow can generate large-scale waves, for example mid-latitude cyclones in the atmosphere. Three components are necessary for baroclinic instability, namely, rotation, stratification and a horizontal temperature (or salinity) gradient.

The source of energy for the disturbances is associated with available potential energy. Available potential energy represents energy which is available for conversion into the kinetic form if the constraints imposed by the equation of motion will allow this to happen. For baroclinic instability, the available potential energy of the basic flow comes from the horizontal temperature gradient $\partial T/\partial y$ [Gill (1982), Pedlosky (1987), Wright (1987)]. Other generation mechanisms that can be significant for instability are wind forcing and flow over topography.

Mathematical models of the baroclinic instability were developed by Charney (1947), Eady(1949), Sutcliffe (1951), Fjortøft (1950), and Phillips (1951). In a number of studies, quasi-geostrophic baroclinic instability models have been used to explain the mesoscale fluctuations observed in various coastal flows [Mysak et al (1981), Wright (1981), Smith (1976), Stanev & Beckers (1999), Stanev & Staneva (2000)].

The stability criterion for the baroclinic waves can be obtained from the equations of motion for a basic flow with small perturbations. For the flow to be stable, the horizontal wave number should satisfy [Kundu (1990), Cushman-Roisin (1994)]:

$$k > 2.399\, f\,/\,NH,$$

where N is the Brunt - Väisäla frequency, H is the depth, and f is the Coriolis parameter.

The corresponding criterion for the wavelength ($\lambda = 2\pi/\,k$) is:

$$\lambda < 2.619\frac{NH}{f} = 2.619R_d.$$

Here R_d is the Rossby radius of deformation, which in continuously stratified fluid is defined as:

$$R_d \equiv \frac{NH}{f}.$$

For the two-layer fluid, the baroclinic Rossby radius of deformation is defined as:

$$R_d = \sqrt{\frac{g\Delta\rho h}{\rho}}\frac{1}{f}. \qquad (1)$$

Here g is the gravitational acceleration, ρ is the density of the upper layer, $\Delta\rho$ is the density difference between the layers, h is the thickness of the upper layer. Thus, the condition for baroclinic instability is that all perturbations of wavelength exceeding 2.619 times the Rossby radius tend to take the system away from the equilibrium. However, in this case the perturbations do not have the greatest growth rate. It can be shown [see for example Kundu (1990), Cushman-Roisin (1994)] that the maximum growth rate can be reached at

$$\lambda_{max} = 3.912\, R_d \tag{2}$$

Waves with length much smaller than the Rossby radius do not grow, and ones much larger than R_d grow very slow. Unstable growing waves also propagate in time in the direction of the basic flow.

Detailed discussion of the baroclinic instability criterion can be found also in the review of Pierrehumbert & Swanson (1995).

In the Black Sea, baroclinic instability is considered to be the main mechanism which generates mesoscale variability. The Black Sea meanders have wavelengths of about 125 km along the western and southern coast and about 250 km along the northern coast [Oguz et al., (1993)]. They are embedded within the overlying circular coastal current (the Rim Current).

Patterns on the surface due to instabilities may take a variety of forms. They can be clearly seen in satellite images as meanders forming loops that may pinch off and form separate eddies (See Figure 3).

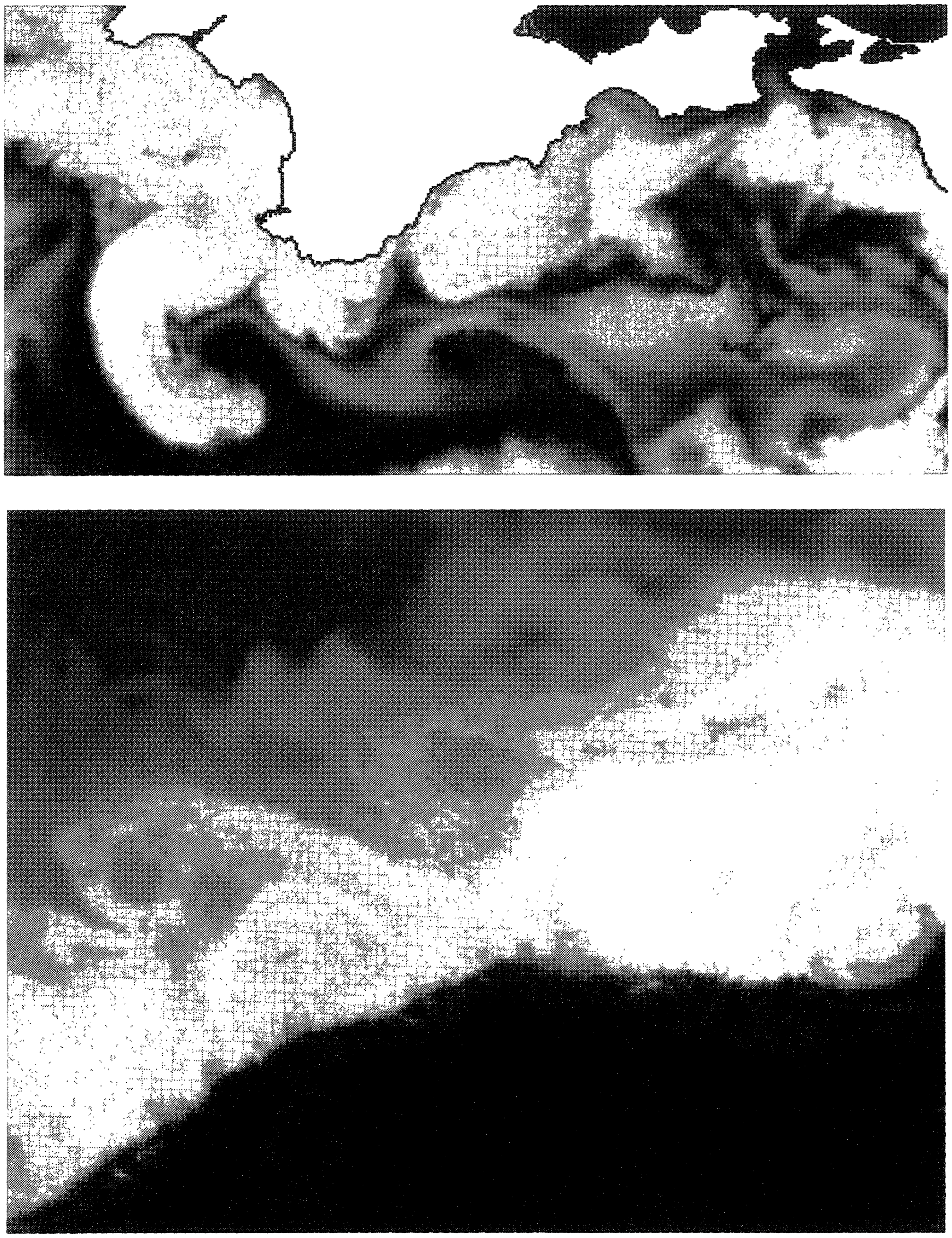

Figure 3. Typical satellite imagery (NOAA IR) of the baroclinic instabilities in different regions of the Black Sea: (a) Crimean peninsula (b) Anatolian coast between 31 and 33° E. Images courtesy of S.V. Stanichny and D. M. Soloviev.

1.4. Research objectives

In the context of achieving a better understanding of the turbulent flow in the oceans in terms of the laws that govern the behavior of vortices and waves and their interaction we set the following objectives:

- To obtain a qualitative understanding of the circulation and the dynamics of the Black Sea, including their coastal and shelf regions.
- To understand the source of the mesoscale variability in the Black Sea.
- To study the structure of mesoscale transient features and how they are affected by the coastline.

1.5. Organization of the Thesis

This work is structured as follows. Following this introductory chapter, Chapter 2 outlines the available data, and the methods (MCC and PIV) applied for the analyses of these data. Results of the data processing and analysis are also specified in this chapter. A description of the experimental setup and results of laboratory modeling are contained in Chapter 3. A brief summary and discussion on the results of this thesis are given at the end of Chapter 2 and Chapter 3.

A complete list of references is presented in Bibliography.

Chapter 2.

Processing of the Satellite Images

2.1 Data overview

A brief description of the data that have been used in this work is presented in this section. The data set available for the present work includes 63 images of the Black Sea. The data were collected from December 1999 to April 2002 by AVHRR (Advanced Very High Resolution Radiometers) aboard the NOAA-12, -14, -15 and -16 satellites and processed in the Marine Hydrophysical Institute (MHI) in Sevastopol (Ukraine). The data have been collected over global equal-angle grids of spatial resolution of 1/100°/pixel per degree of longitude and 1/70°/pixel per degree of latitude. Pixels have equal west-east and north-south separations of ~1.1 km. There are 801 lines in the images, each with 1501 pixels.

A typical example of the satellite images is shown in Figure 5. Almost all of the 63 original satellite images were partially cloud-covered. All available images allowed us to compose 43 pairs of consecutive images suitable for analysis. However, in view of the fact that we are limited with respect to the time interval between images and the quality of images regarding their cloud covering, the real number of the processed images did not exceed 15 pairs. A list of the image pairs is given in Appendix 1.

Figure 4. A typical example of the used satellite images (4 October 2001).

2.2. PIV and MCC methods

The remote sensing techniques can provide a wealth of information on the ocean surface velocity fields at a high level of spatial and temporal resolution. Although satellite altimetry can be very informative, there exist limitations of its applicability. For example, because of the geoid uncertainties, normally it cannot be used on shelves or in shallow regions. The most popular alternative technique for reconstructing velocity fields in the flow is the Maximum Cross Correlation (MCC) method described in Emery et al. (1995), which derives the advective velocity fields from the spatial pattern displacements in sequential pairs of satellite (normally infrared) images.

In this procedure, the displacements of small regions of the patterns of passive tracers are estimated between sequential images using cross correlations between small rectangular sections from each image. Applied to infrared sea surface temperature (SST) images, the MCC method tracks displacements of SST where there is no upwelling or strong surface heating.

Similar techniques are widely used in experimental fluid dynamics. Collectively these techniques are known as Correlation Imaging Velocimetry [see, e.g., Fincham and Spedding, (1997)]. The name Particle Imaging Velocimetry (PIV) is commonly used when small particles of neutral density are seeded in the fluid. However, any passive tracer that provides image texture and follows the flow may be used. The scalar field of sea surface temperature (SST) is often used for oceanographic applications. SST is generally not a passive tracer though, because of heating and cooling at the surface. The lack of conservation of temperature applies additional restrictions on the choice of pairs of SST images (nighttime, intervals of only a few hours) to be used for the analysis and interpretation of the results obtained. MCC generally gives poor results when used to estimate the velocities along the front of the scalar field due to poor correlations if there is no contrast pixel patchiness along the front. This is a serious disadvantage of the method although it can be reduced somewhat by application of objective interpolation technique using dynamical constraints.

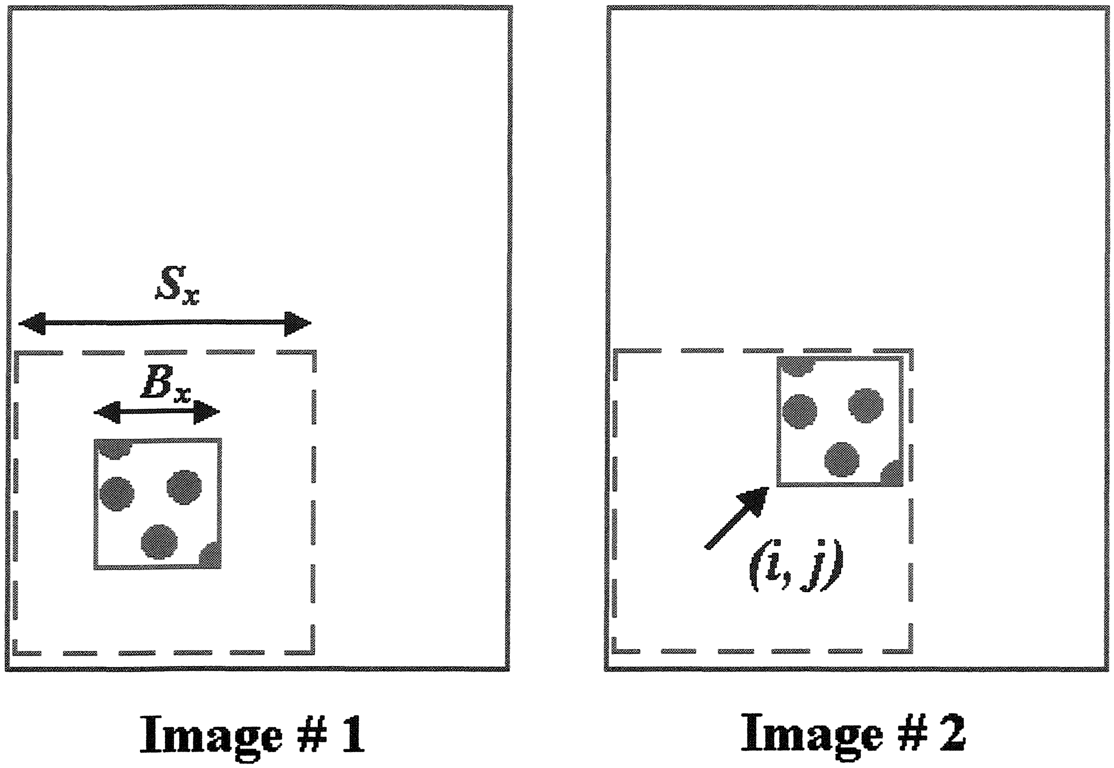

Figure 5. A search for cross-correlations between two images. (i, j) - displacement vector, B_x - size of pattern box, S_x - size of search window.

Initial processing of the pairs of satellite images was performed using software originally developed for PIV analysis. A description of the algorithm is given by Pawlak and Armi (1998). In this procedure two consecutive images with time difference Δt are considered. The first image is divided into small pattern boxes of size B_x by B_y. Each pattern box may move in any direction, but the displacement of the box (i, j) is restricted by the maximum possible flow velocity. The displaced position is searched within a search window S_x centered at its current position in the second image (Figure 5). The cross-correlation function $c(i, j)$ between two images is calculated for all possible locations inside the search window:

$$c(i,j)=\frac{\sum_{k=1}^{B_x}\sum_{l=1}^{B_y}(I_a(k,l)-\bar{I}_a)(I_b(k+i,l+j)-\bar{I}_b)}{\left[\sum_{k=1}^{B_x}\sum_{k=1}^{B_y}I_a(k,l)-\bar{I}_a)^2\sum_{k=1}^{B_x}\sum_{k=1}^{B_y}(I_b(k+i,l+j)-\bar{I}_b)^2\right]^{1/2}}$$

I_a, I_b - pixel intensities of a pattern box of size B_x by B_y, $\bar{I}_a$, $\bar{I}_b$ - mean intensities.

$$\bar{I}_a=\frac{1}{B_xB_y}\sum_{k=1}^{B_x}\sum_{l=1}^{B_y}I_a(k,l)$$

$$\bar{I}_b=\frac{1}{B_xB_y}\sum_{k=1}^{B_x}\sum_{l=1}^{B_y}I_b(k+i,l+j)$$

The position of the maximum cross-correlation coefficient gives the nearest integer displacement of the pattern box in the second image. Sub-pixel accuracy of the displacement is obtained by fitting a Gaussian function to the correlation peak, and finding the exact peak location (Figure 6) [Fincham and Spedding, (1997)].

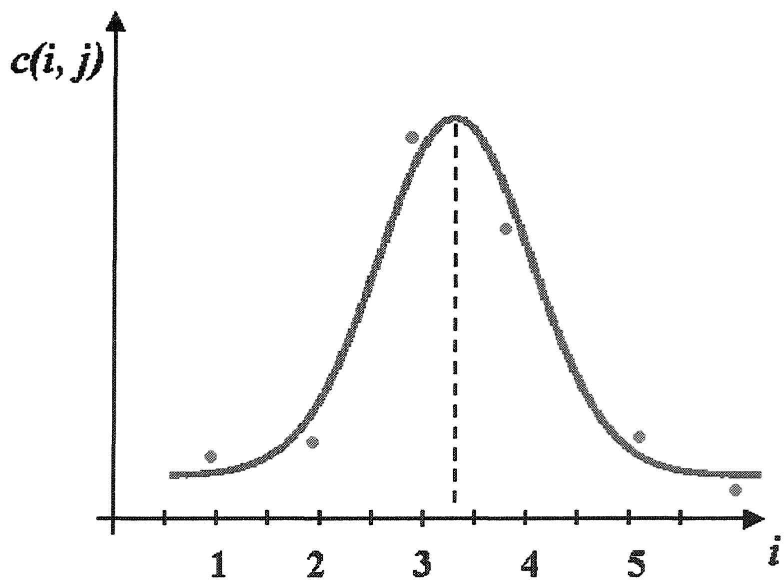

Figure 6. A search for the correlation peak with sub-pixel resolution.

The change in location is considered to be the water particle displacement, which then allows velocity to be calculated. The MCC method can detect sub-pixel resolution displacement of water motion vectors. For the satellite imagery we use, the accuracy is usually between 1/3 and 1/2 pixel displacements.

We used square regions of 12 by 12 pixels, at intervals 6 pixels in both directions. These sections were small enough to resolve the mesoscale features of a size of approximately 30 km. On the other hand, the correlation region was large enough to contain a number of small-scale distinctive features, which create the texture of the image.

This method applies to each pair of images with time difference between them not less than 180 min and not more than 800 min. Analysis of the available pairs of images showed that this particular time interval between the images is optimal for the MCC procedure. Temperature is approximately conservative over this time interval, while water parcels move an appreciable distance (1–3 pixels). To resolve a displacement of 1 pixel of water parcels with speed ~10 cm/s on an image with space resolution ~1.1 km/pixel, the time between two successive images should be not less than 180 minutes. If the time between two images is too short, it leads to the detection of only fast moving parcels and to the overestimation of the velocity field. If the time interval between images is too long, the distinctive parts of the first image shift so far-off that the correlation cannot be found. If a displacement exceeds the comparable areas (is larger than 20 pixels), the MCC method cannot detect correlations properly. The minimum velocities that can be detected at different times between images are presented in Table 2.

Table 2. Dependence of the minimum velocity, which can be detected by PIV/MCC method, on the time between images.

Time between images, min	Minimum velocity, cm/s
50	38
100	19
200	9
600	3

The processing of images and analysis of the correlations were performed using MathWorks Matlab and the Image Processing Toolbox.

We tested the Matlab code we used a few pairs of images of the same size as all available satellite images (1051 by 801 pixels) with a simple geometry and *a priori* known displacements. Results of calculations confirm the accuracy of the applied code. One of the examples of testing calculations is presented in Figure 7. Two successive images with a displacement of 1 pixel (Fig 7a) and 20 pixels (Fig. 7b) in the southeastern direction were considered. The results demonstrate that the code is less sensitive to relatively big patches with dimensions larger than 80 by 80 pixels (areas 1 in Fig. 7a, and 2 in Fig. 7b). If the time between images is too big (greater that 800 min) and displacement exceeds the size of 12-by-12 cells, the code is unable to catch all movement and even some improbable motions may appear. (See area 1 in Fig. 7b)

After applying the PIV/MCC methods, we obtain the intervening velocity fields calculated at each point on an 85 by 64 (13.5 by 13.5 km) grid for each pair of successive images.

To prove the accuracy of the technique, one more test was used. Every pair of successive images has been subjected to manual comparison.

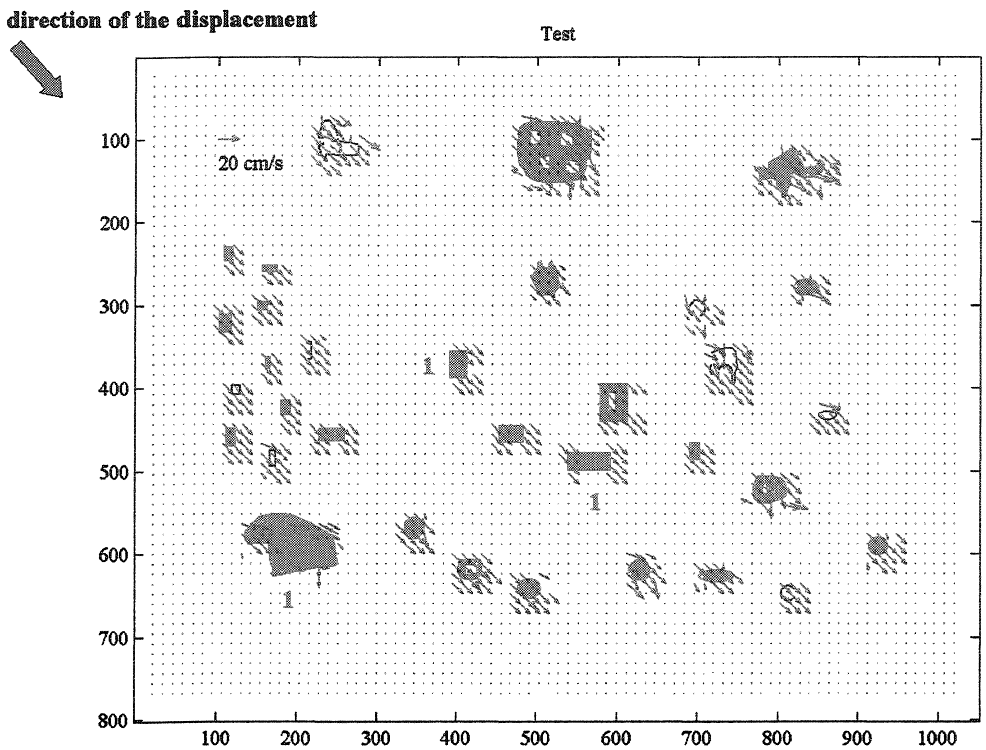

Figure 7a. A test for PIV&MCC Matlab code. Displacement of 1 pixel was applied in the southeastern direction; time between 2 images 200 minutes, velocities ~ 15 cm/s.

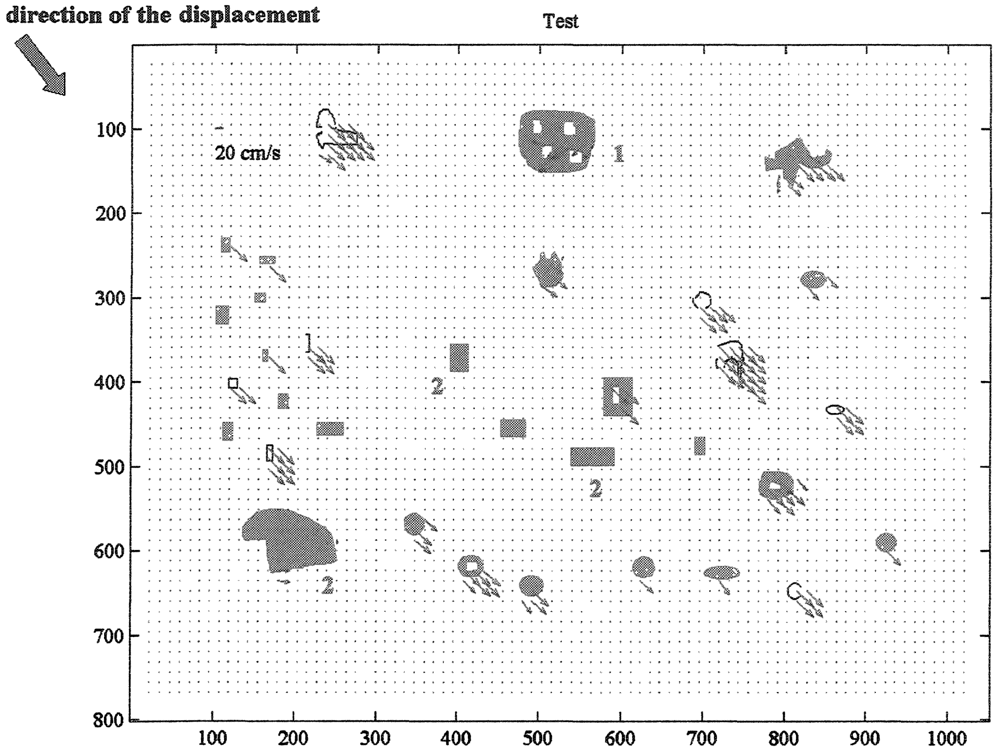

Figure 7b. A test for PIV&MCC MatLab code. The same initial image was displaced on 20 pixels in the southeastern direction; time between 2 images 900 minutes, velocities ~ 40 cm/s.

2.3. Filters

While AVHRR provides complete satellite coverage of the Black Sea area, the presence of clouds obscures the surface in the near-infrared channel. This is the main limitation with using AVHRR data for acquiring velocity fields.

A few filters to the images and computed velocity fields have been applied to remove "obscured" areas and "unphysical" vectors.

The first filter eliminates the areas covered by clouds, choosing " obscured " areas of uniform black color. The following procedure is applied to every image independently. Each cell of size 12-by-12 pixels is examined for the presence of the black color that corresponds to cloud coverage. If at least one pixel of the cell contains a cloud, then the whole cell is removed and is not processed.

The next two filters are used to remove of casual vectors that may appear due to false correlations. Assuming the water moves locally and uniformly without sudden changes in velocity direction and magnitude, the filters are used to compare each vector with 8 neighboring vectors to check the smoothness, spatial coherence and magnitude.

For each computed velocity vector $\vec{V}(i, j)$ the smoothness filter tests the difference (U_m, V_m) between its horizontal components $U(i, j)$, $V(i, j)$ and the average values and of the encircling cluster of 8 vectors, i. e.

$$U_m = U(i,j) - \left[\frac{U(i-1,j-1)+U(i-1,j)+U(i-1,j+1)+U(i,j-1)}{8} + \frac{U(i,j+1)+U(i+1,j-1)+U(i+1,j)+U(i+1,j+1)}{8}\right];$$

$$V_m = V(i,j) - \left[\frac{V(i-1,j-1)+V(i-1,j)+V(i-1,j+1)+V(i,j-1)}{8} + \frac{V(i,j+1)+V(i+1,j-1)+V(i+1,j)+V(i+1,j+1)}{8}\right].$$

We assume that the maximum difference between two adjoining vectors cannot exceed 20 cm/s. If the difference U_m or V_m is greater than the specified threshold value U_{th} or V_{th} respectively, the vector $\vec{V}(i, j)$ is considered to be "unrealistic" and is replaced by the median value of 8 encircling velocities.

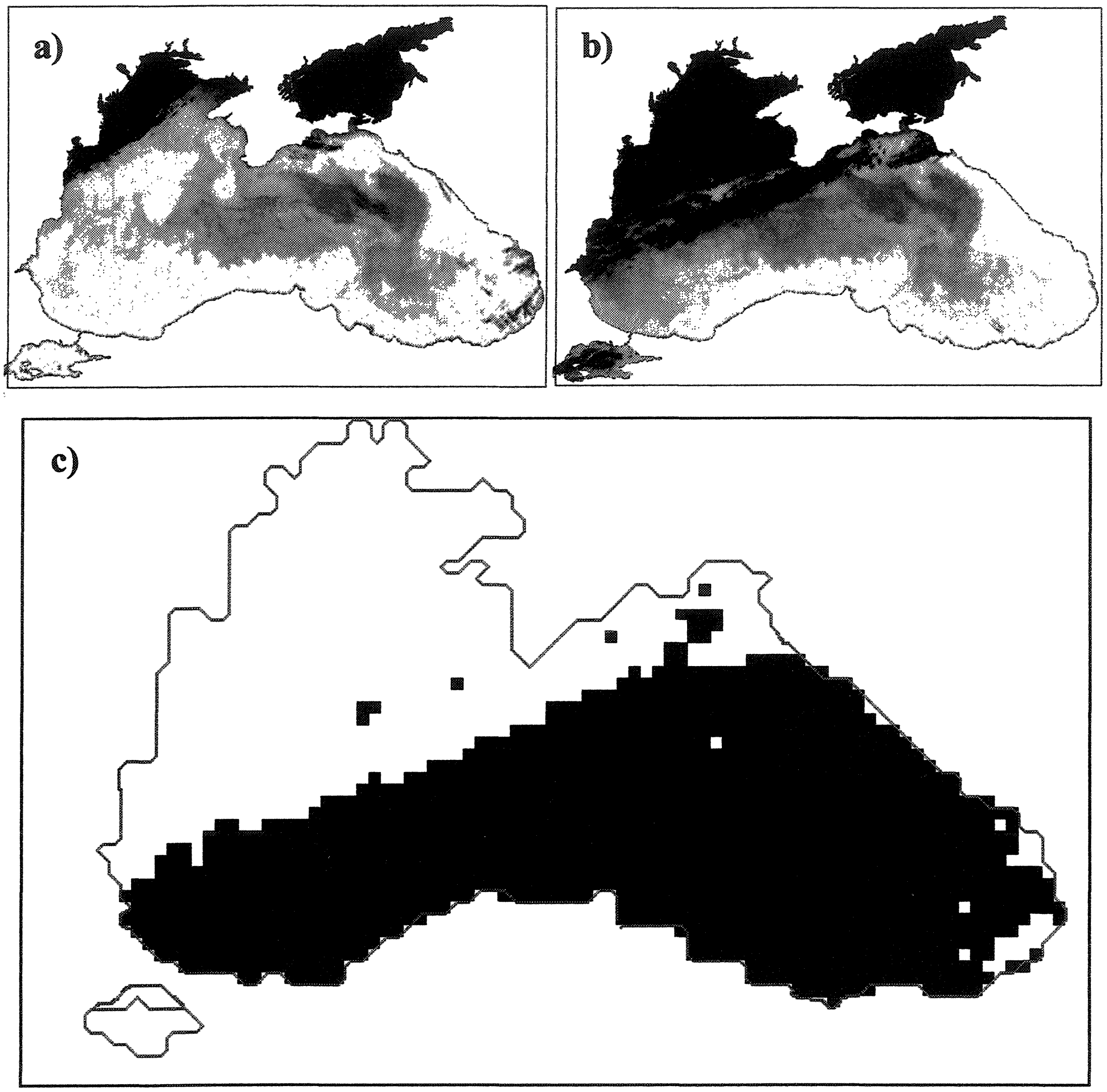

Figure 8. a) and b) typical example of two successive images (size 1051by 801 pixels) partially covered by clouds. In c) - the black area represents the resulting image part, which was processed by MCC method after eliminating clouds (size 85 by 64 pixels). A blue line shows the coastline of the Black Sea.

Observations show that on the sea surface there is no mesoscale motion that exceeds say 80 cm/s. The magnitude filter compares the magnitude of each calculated vector

$\vec{V}(i,j)=\sqrt{U(i,j)^2+V(i,j)^2}$ with the maximum acceptable velocity V_{max}. Any detected vector with the magnitude greater than V_{max} is considered to be "unphysical" and is removed. Cloud contamination is the main reason for eliminating vectors. Cloudiness is more persistent and frequent during the winter, resulting in fewer vectors from AVHRR. After applying the filters, the grid on which velocities have been calculated becomes irregular with gaps in the areas covered by clouds. The total number of calculated velocities differs from 2298 to 1353 depending on the percentage of the cloud coverage (from 1 to 23%).

2.4. The variational method

We used the variational method [Panteleev et al. (2002)] to interpolate the velocity field obtained by PIV/MCC. The basis of this method is to apply appropriate dynamical constraints to the original velocity field. The obvious advantage of the MCC method, on the other hand, is that this method provides nearly instantaneous estimates of the currents over a large area (over the large portion of the Black Sea in our case). It is difficult to obtain this important information on the surface layer dynamics over all regions of the sea by any other means.

The variational method is designed to determine a stationary two-dimensional circulation from estimates of horizontal velocities by minimizing the functionals which represent the sum of different hydrodynamical constraints I_i on the flow field:

$$F=\sum_{i=1}^{n} I_i\,,$$

where n - the number of constraining parameters.

We used in particular the following integral constraints:

$$I_1 = \iint \frac{u_{xx}^2 + u_{yy}^2 + v_{xx}^2 + v_{yy}^2}{g_1} dxdy;$$

$$I_2 = \iint \frac{u_x + v_y}{g_2} dxdy.$$

Here I_1 and I_2 are the smoothness and the divergence of the velocity field (u, v), respectively.

$$I_3 = \sum_{k=1}^{N} (\vec{U} - \vec{U}_k^*)^2 / g_3,$$

where U_k^* - initial input velocities, N - the total number of the input points.

Constraint I_3 expresses the correspondence of the calculated velocities to original input data. The values of the weight functions g_i were chosen to produce a smooth and almost divergence-free flow field keeping the correspondence with the original and modified data within reasonable limits. The choice of appropriate values for the coefficients g_i presents the main challenge of the method. Thirty five different combinations of weight coefficients g_i were examined in this work. Five of them giving the most differing resulting fields are presented in Table 3. In Figure 9, velocity fields calculated for these sets of coefficients are shown. Calculations demonstrate that the resulting velocities are not highly sensitive to the choice of weight coefficients. The maximum difference of the final velocity vectors calculated for different values of g_i does not exceed 30° in vector direction and is negligible in the magnitude (Figure 9). Thus, the decision to use the one or the other set of possible values is the compromise between the smoothness of the outcome data and their agreement with input velocities.

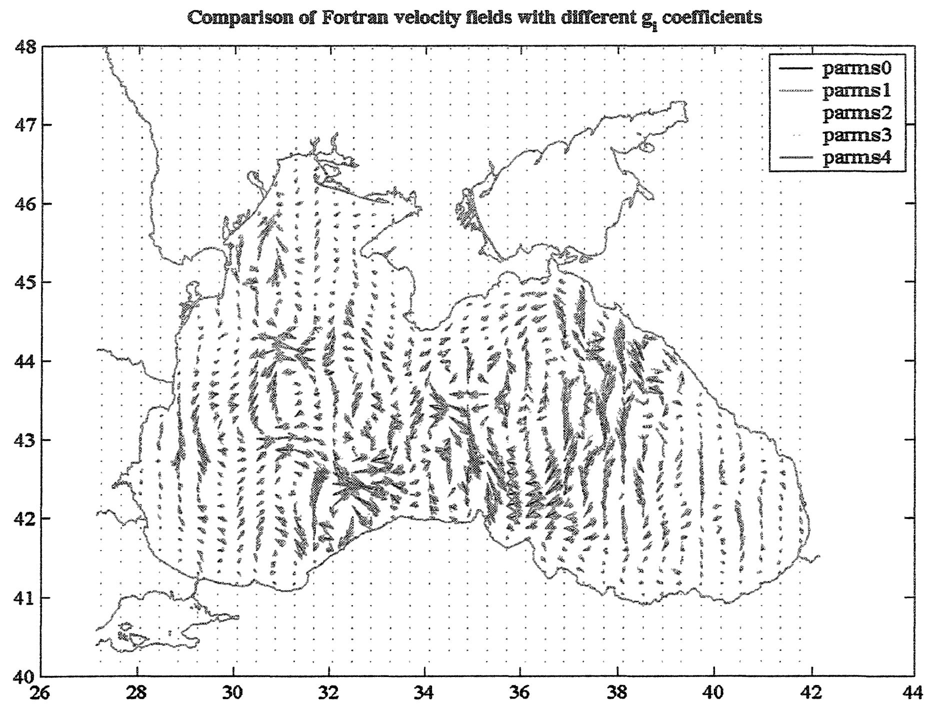

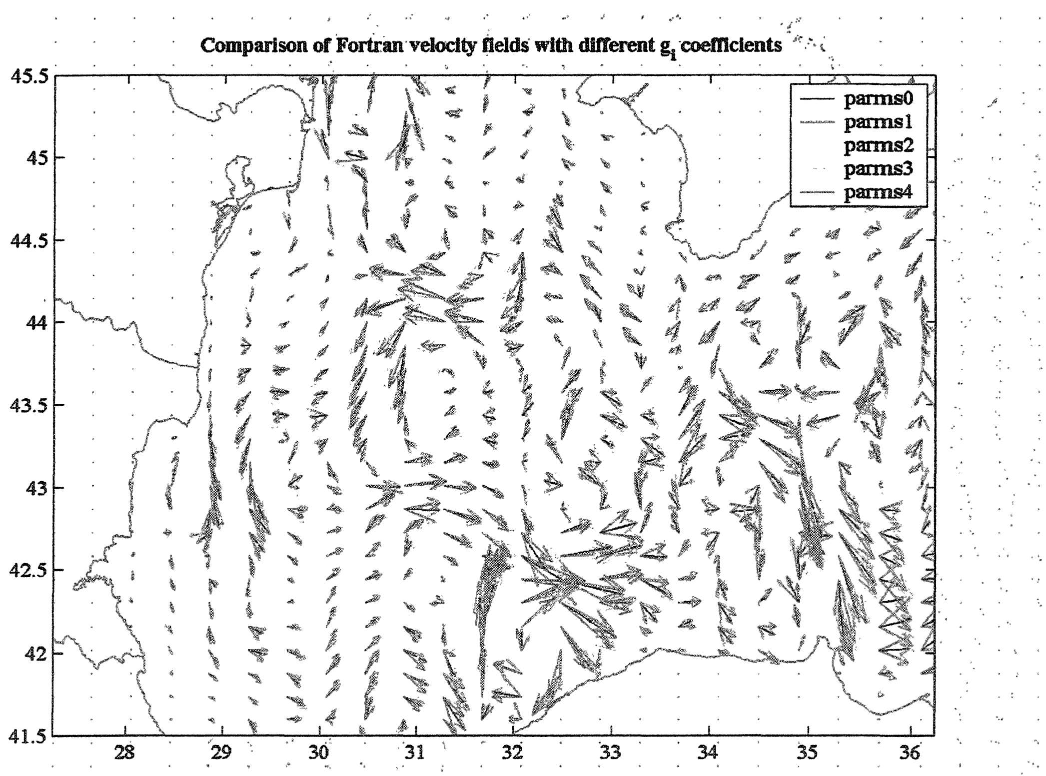

Figure 9. Dependence of a form of the velocity field on the values of weighing coefficients g_i. The values for different sets of g_i coefficients (parms 1 - parms 4) are given in Table 3.

Table 3. Some values which have been used for weighing coefficients g_i

Coefficient	Parms0	Parms1	Parms2	Parms3	Parms4
g_2	5	50	70	100	100
g_1	0.5	10	10	10	5
g_3	0.3	30	30	0.5	0.5

The program software was written in Fortran code. As initial input data, the horizontal velocities on the irregular grid obtained after PIV/MCC method were used. The minimum of function F was reached after about 500 - 600 iterations. The realistic coastline was also taken into account in these calculations. The resulting velocities were calculated on a 74-by-56 grid giving grid cells of 16 by 15.5 km. The Fortran code was also tested for a generated simple velocity field (Figure 10).

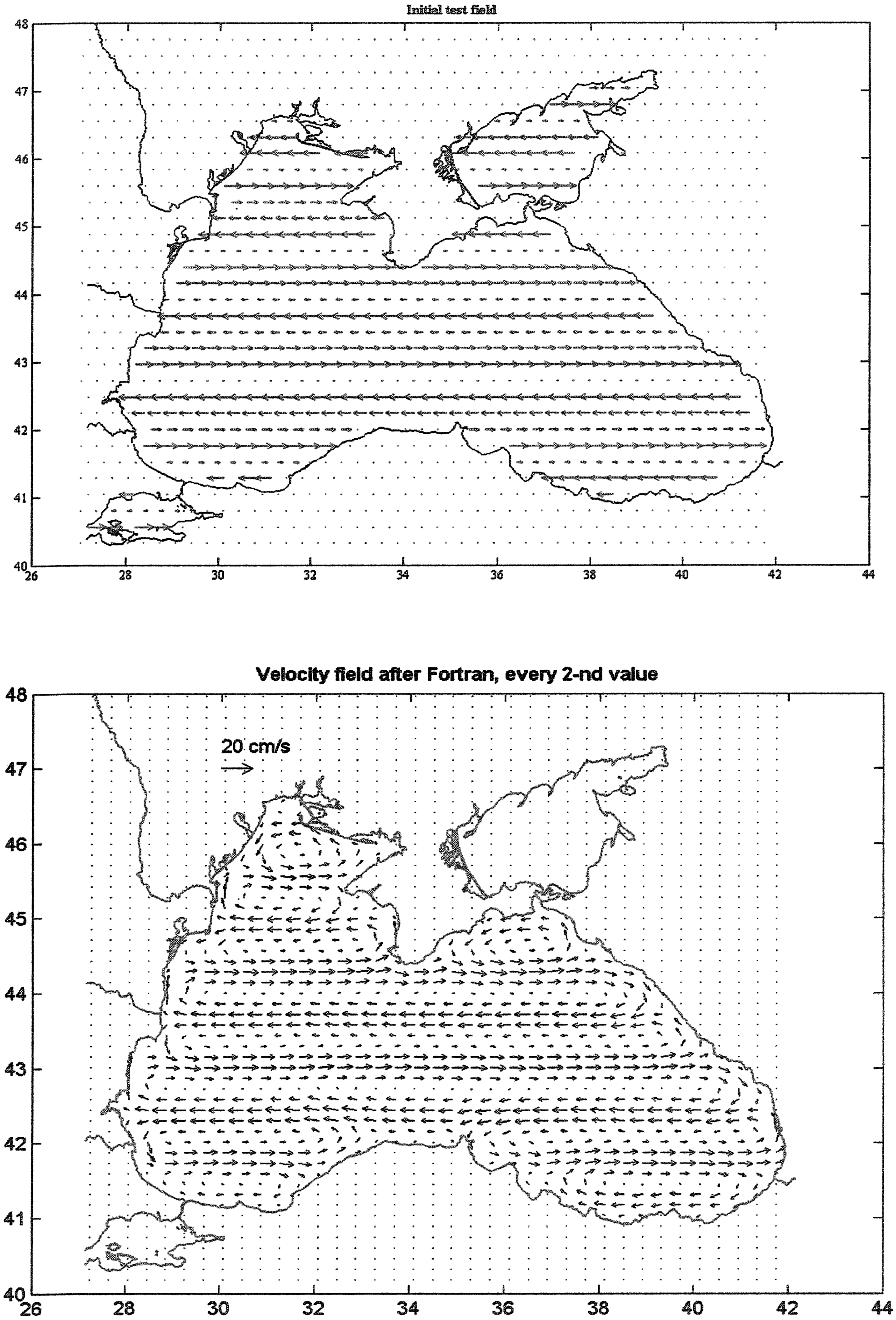

Figure 10. A test of the Fortran code. No sink or sources at the shore, velocity is zero out of the sea. **a)** Initial velocity field, **b)** Velocity field obtained after applying the variational method.

The velocity field obtained by the application of the MCC procedure and the modified velocity field obtained by further application of the interpolation/smoothing procedure are shown in Figure 11 for comparison.

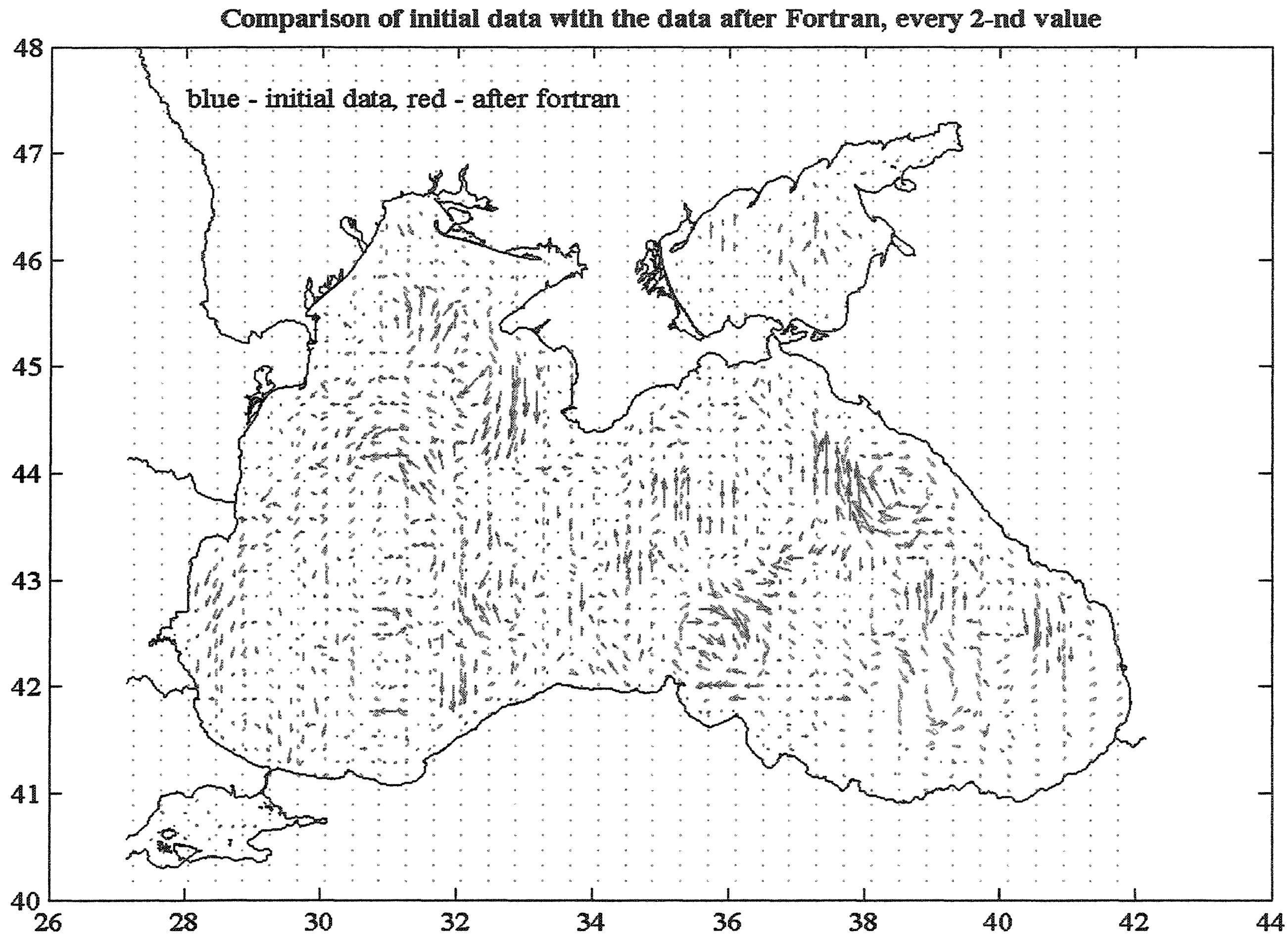

Figure 11. Comparison results obtained after using Matlab and Fortran codes for June 15, 2001. Red arrows reproduce the velocity field obtained after applying the PIV/MCC method (the MatLab code), blue arrow show the velocity field improved by using the variational method (the Fortran code)

2.5. Results and discussion

This section describes the surface circulation of the Black Sea based on the results of applying the PIV\MCC and variational methods.

The upper layer waters of the Black Sea are characterized by a predominantly cyclonic, strongly time-dependent and spatially-structured basinwide circulation. The predominant features of the circulation at seasonal time-scales have been identified.

Our results reveal a complex, eddy-dominated circulation with different types of structural organizations of the interior cyclonic gyre as well as meanders, filaments, and eddies of the Rim Current (Figure 12). The interior circulation is composed of an interconnecting series of cyclonic eddies, and sub-basin scale gyres, varying in size and shape across the basin. They evolve continuously by interactions among each other, as well as with the Rim Current. A series of anticyclonic eddies confined between the coast and the meandering Rim Current zone are the products of the mesoscale variability.

The velocity fields show a remarkably persistent signature of the seasonal flow structure, examples of which are shown in Figure 12 (a - d) for December, April, June and November for the years 1999 - 2002.

The most distinctive feature of the winter and spring circulation is a strong salient boundary current - the Rim Current (see Figures 12b, 12d). The strong cyclonic circulation caused by intense prevailing winds is accompanied by rather weak anticyclonic peripheral recirculation. Such persistent eddies as the Batumi and Sevastopol are noticeable and strong, though. In summer months, the circulation is subject to essential weakening. The Rim Current weakens and almost disintegrates into smaller - scale cyclonic features (Figure 12c). The width of the Rim Current manifests the strong variability. It is almost twice as wide during the winter - spring season than in the summer - fall, oscillating from 40 km in June - September to about 100 km in December - April. Seasonal dependence of the Rim Current width is presented in Figure 15 and Table 4. The velocity of the Rim Current is also subject to significant seasonal changes. It has its maximum in April reaching in some places 50 cm/s and decreases to 15 cm/s in September. These results agree with direct observations [Blatov et al. (1984)], altimetric data [Korotaev (2001), Korotaev et al. (2003)] and numerical simulations [Oguz & Malanotte-Rizzoli (1996)]. Such behavior may be explained by the consolidated influence of two main driving forces: wind and river discharge which reach their minimum in August - September. Fresh water supply has its maximum in April when wind forcing is still very strong.

Numerous baroclinic eddies and meanders are clearly seen, especially during the summer - fall season, along the Anatolian coast and near the Bosphorus Straight. Their formation can be explained by a strong fresh water supply in the northwestern part of the sea. Experimental confirmation of such an approach is presented in Chapter 3.

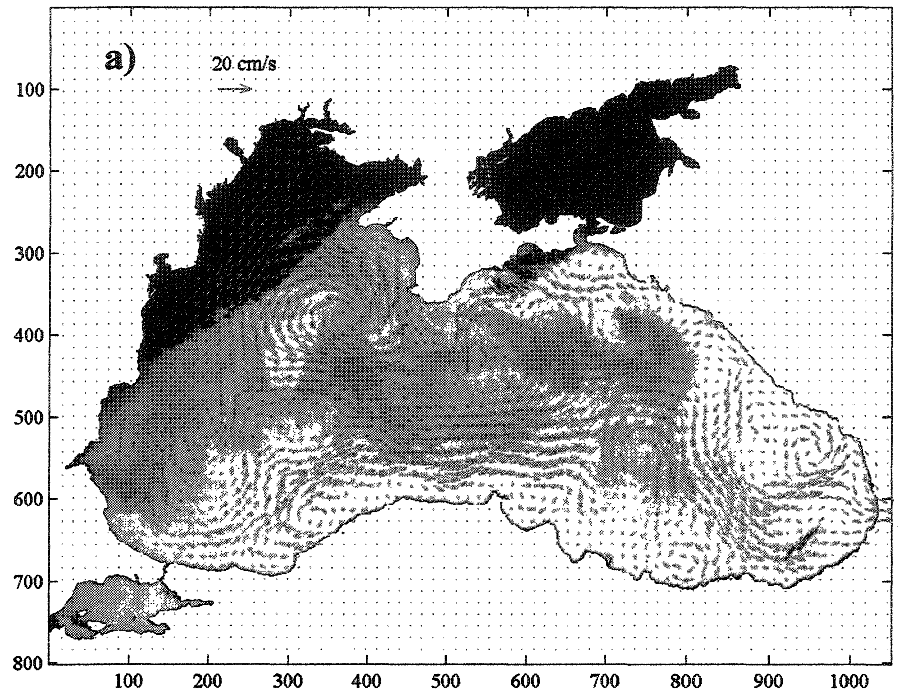
a)
20 cm/s
100
200
300
400
500
600
700
800
100
200
300
400
500
600
700
800
900
1000

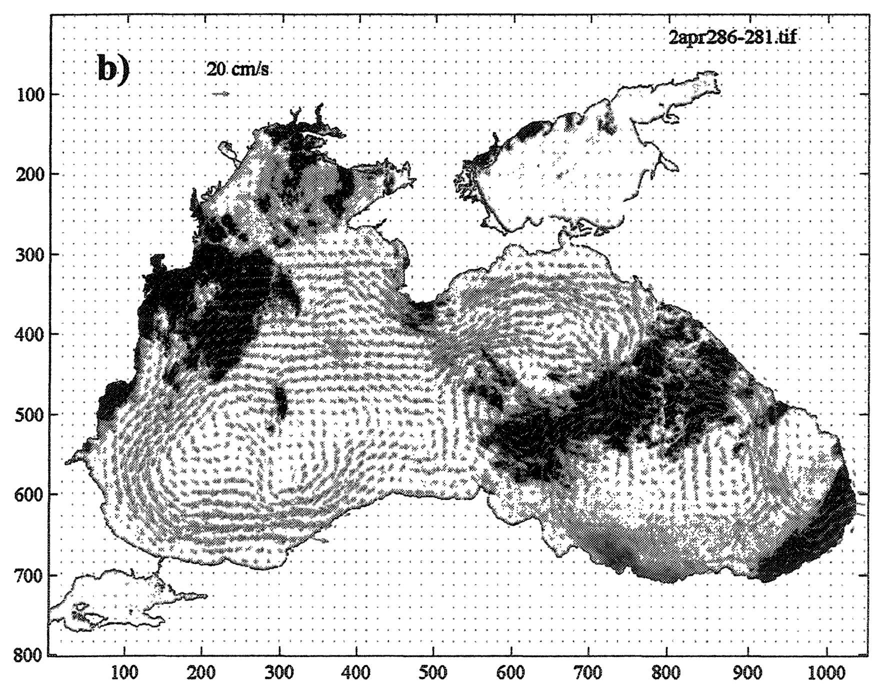
b)
20 cm/s
2apr286-281.tif
100
200
300
400
500
600
700
800
100
200
300
400
500
600
700
800
900
1000

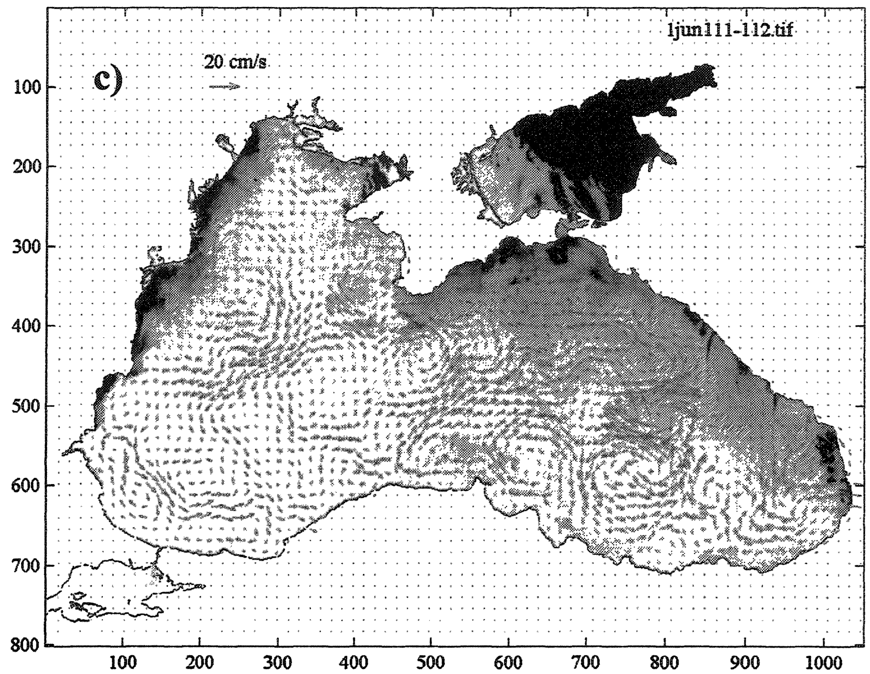

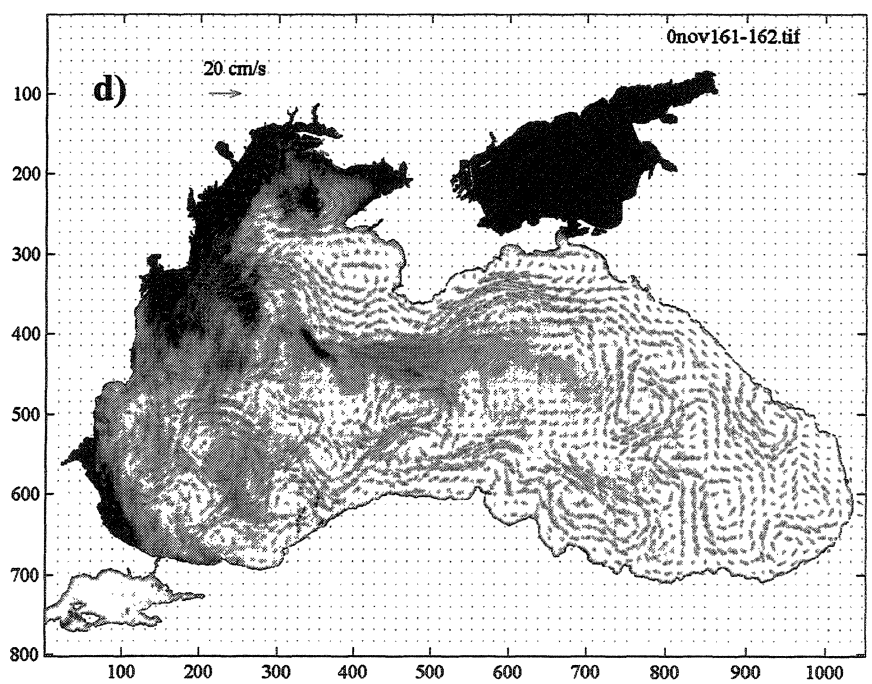

Figure 12. Seasonal variability of surface circulation of the Black Sea. Velocity fields are given for all for seasons: a) December 2, 1999, b) April28, 2002, c) June 11, 2001, d) November 16, 2000.

Table 4. Seasonal dependence on the number of eddies and the Rim Current width

Month	Total number of the eddies	Number of anti-cyclonic eddies	Number of cyclonic eddies	Rim Current width, km
January	41	23	18	70.15
March	40	21	19	-
March	45	24	21	94.35
April	37	18	19	105.23
May	56	28	28	93.54
June	58	27	31	58.46
June	61	31	30	40.92
July	67	35	32	52.61
September	55	30	25	-
September	58	32	26	46.77
October	57	31	26	70.15
October	61	30	31	81.84
October	53	30	23	-
November	45	28	17	87.69
December	41	22	19	81.84
December	31	17	14	99.38

For the interpolated velocity fields calculated using the Fortran code the vorticity was calculated by the following scheme:

$$w(i,j) = \frac{[V(i,j+1)+V(i-1,j+1)+V(i+1,j+1)-V(i-1,j-1)-V(i,j-1)-V(i+1,j-1)]}{6V_{x\_res}\times xstep\times f_{Cor}} + \frac{[U(i-1,j)+U(i-1,j+1)+U(i-1,j-1)-U(i+1,j+1)-U(i+1,j)-U(i+1,j-1)]}{6V_{y\_res}\times ystep\times f_{Cor}}$$

where i = 1:56, j = 1:74 - the numbers of rows and columns (see Figure 13); $V_{x\_res} = x(1, 2) - x(1, 1)$; $V_{y\_res} = y(2, 1) - y(1, 1)$ - the distance in pixels between two adjacent cells for which velocities were calculated; $xstep = 1/100 \cdot 111.423 \cdot 10^5$ cm - the number of cm in 1 pixel in the x-direction, $ystep = 1/70 \cdot 80.141 \cdot 10^5$ cm - the number of cm in 1 pixel in the y-direction, 111.423 km and 80.141 km correspond to 1° of longitude and latitude respectively at 43° N. latitude, 1/70 degree and 1/100 degree - the spatial resolution of longitude and latitude, respectively. The vorticity was nondimensionalized by the Coriolis parameter $f_{Cor} = 1.01 \times 10^{-4}$ s^{-1} estimated for the latitude of 43°.

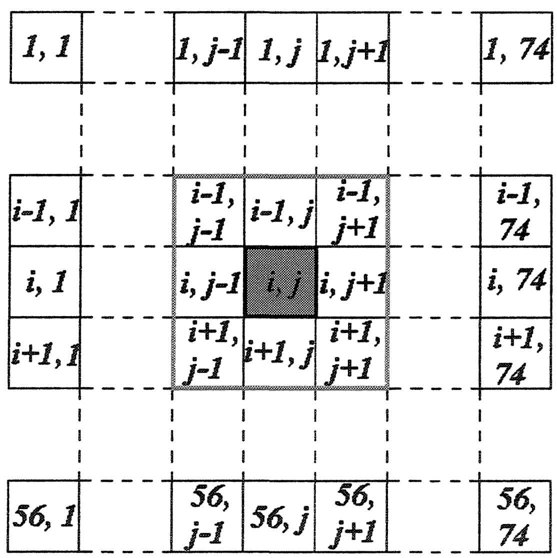

Figure 13. The grid used in the Fortran code on which velocities and vorticities were calculated.

The number of vortices increases during the summer - fall season, but their size and amplitude decrease. Besides slightly predominant anticyclonic activity is observed for all seasons (Figure 14 and Table 4). The winter intensification of circulation can be explained by intensification of wind forcing during this period.

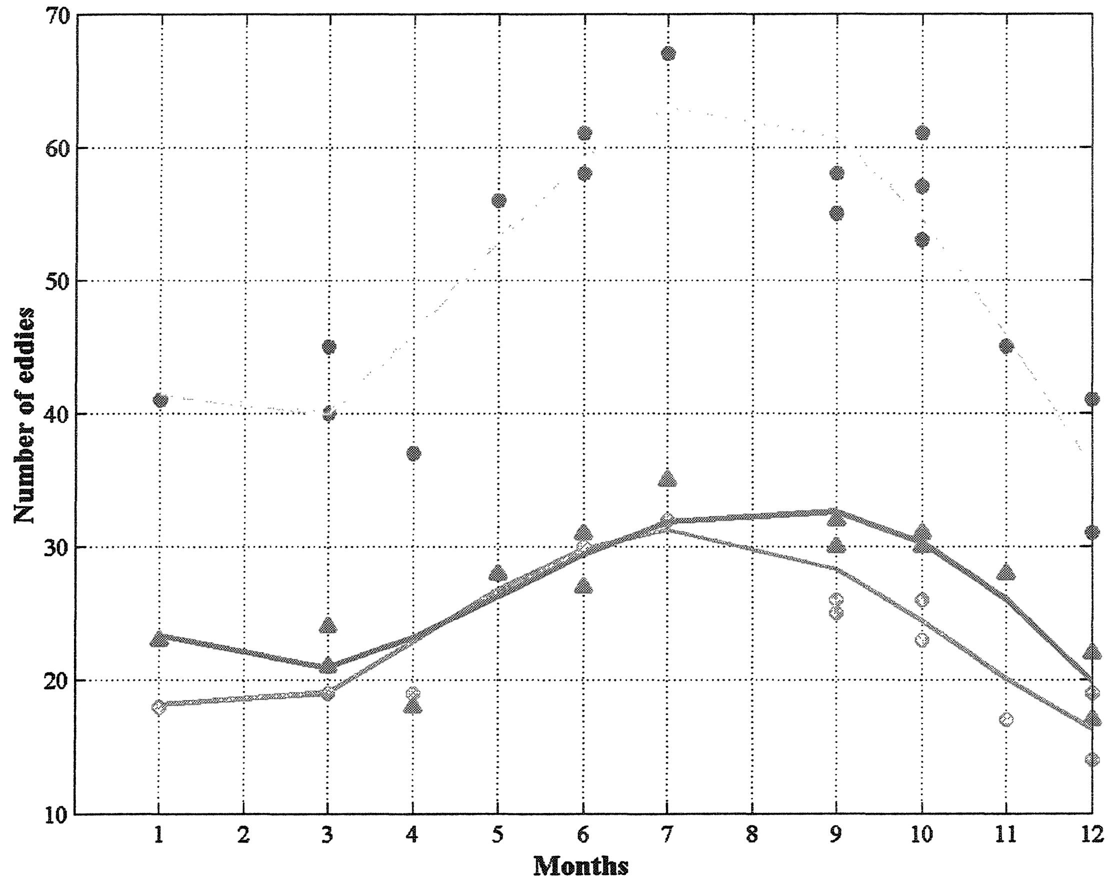

Figure 14. Seasonal dynamics of the eddy number. The total number of eddies is shown by blue dots. The cyan line corresponds to the polynomial curve fitting. The red line and triangles show anticyclonic eddies with corresponding polynomial curve fitting. The magenta line and circles stand for cyclonic eddies.

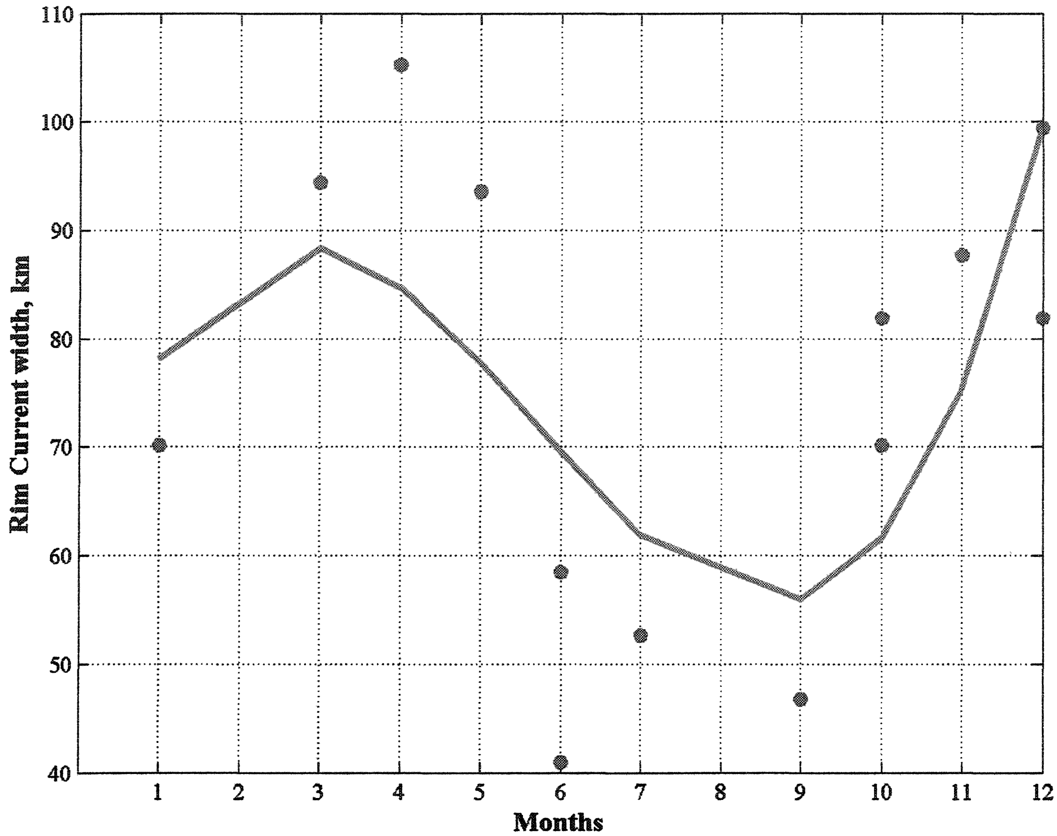

Figure 15. Seasonal variability of the Rim Current width. The red line corresponds to the polynomial curve fitting.

Vorticity field

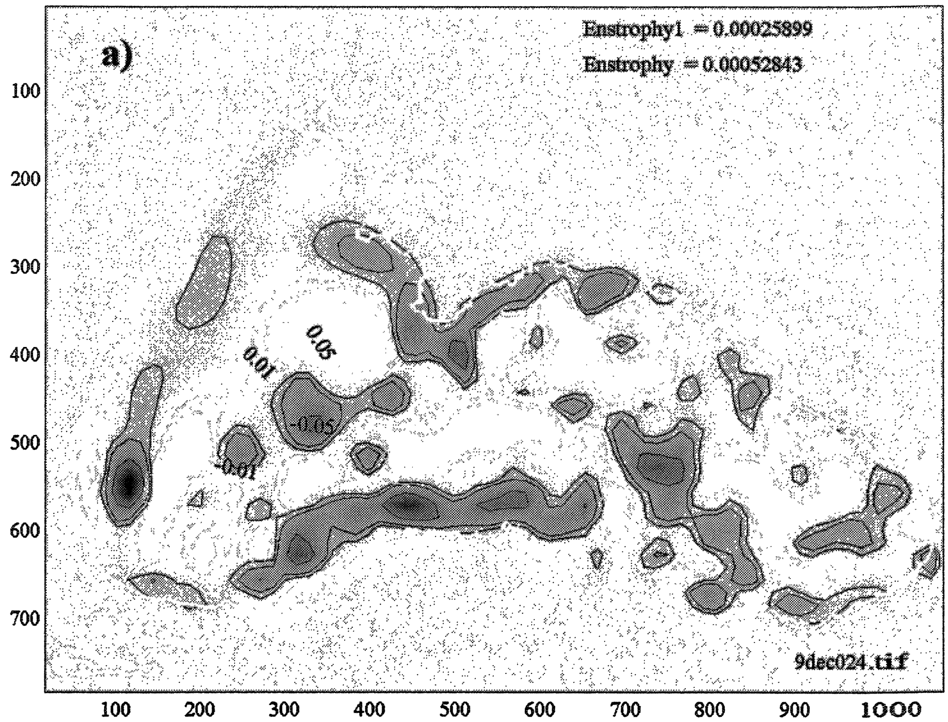

Vorticity field

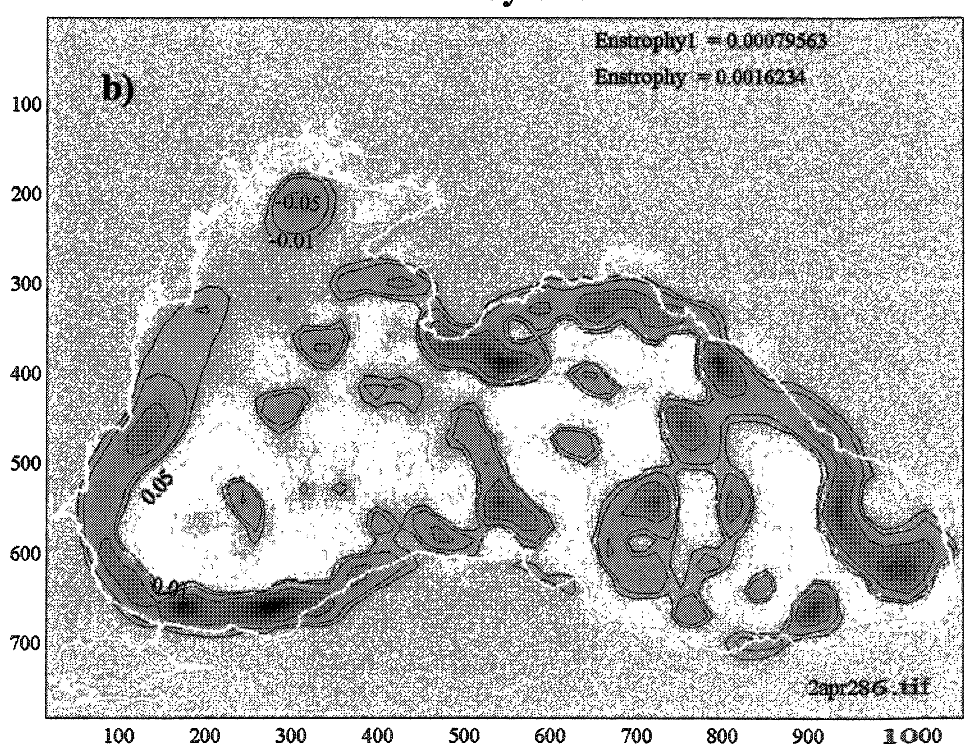

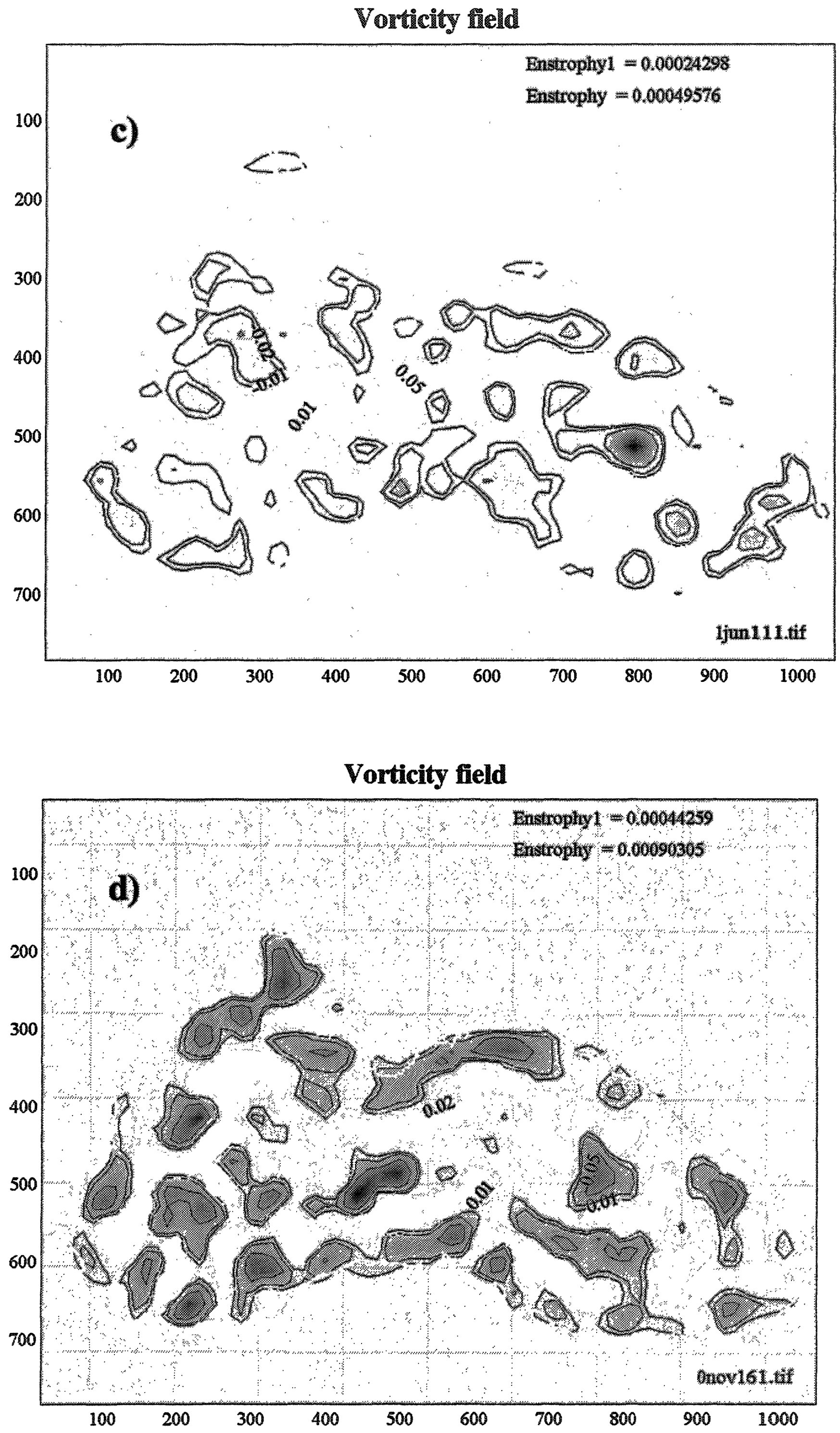

Figure 16. Seasonal variability of the vorticity field. a) December 2, 1999, b) April 28, 2002, c) June 11, 2001, d) November 16, 2000. Vorticity contours are given for the values ± 0.01, ± 0.03, ± 0.05. White and black lines represent cyclonic and anticyclonic vorticity, respectively.

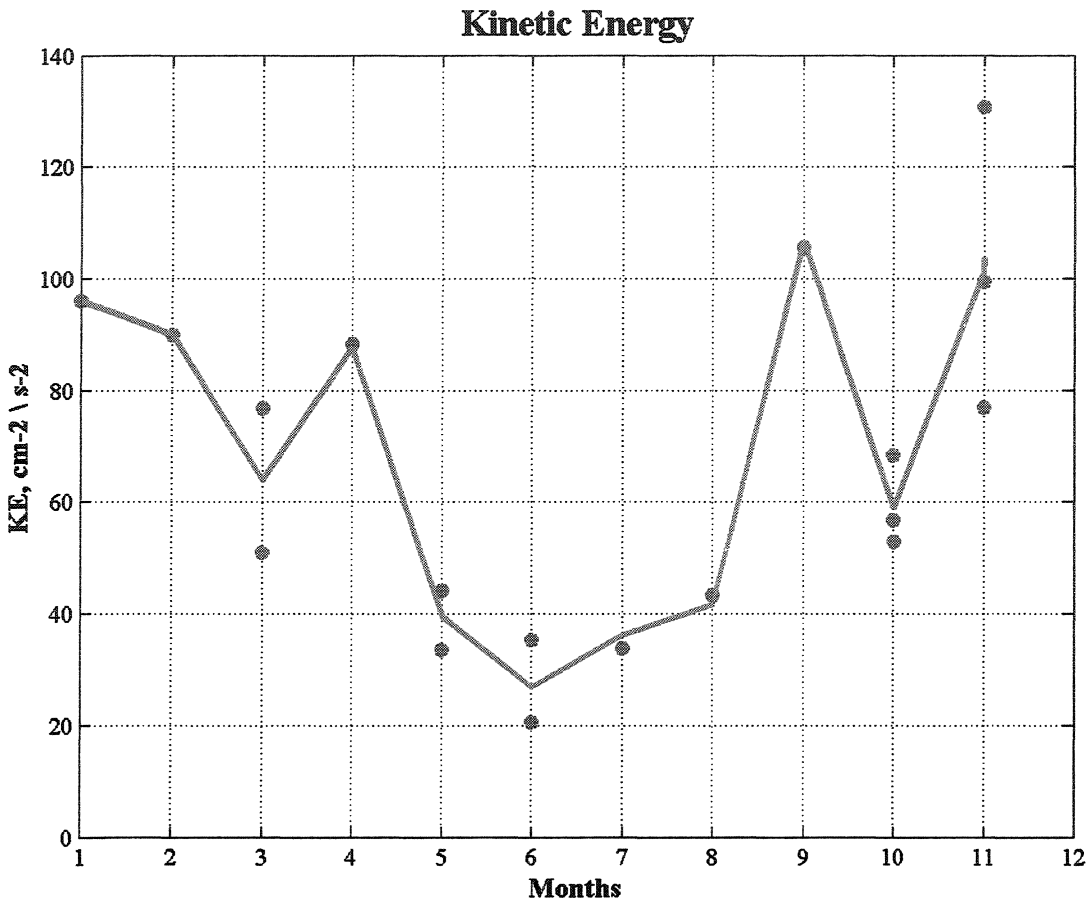

Figure 17. Temporal evolution of the basin-averaged kinetic energy. The red line represents a polynomial curve fitting.

The average kinetic energy over the basin is given by:

$$KE = \frac{\sum_{i=1}^{N}(U_i^2 + V_i^2)}{2N},$$

where U_i, V_i are the horizontal components of velocity vector, $N = 1778$ is the total number of the points where velocities were calculated. The temporal evolution of the kinetic energy KE is presented in Figure 17 and Table 5.

Maximum values of the kinetic energy are reached in the winter - spring season, and the minimum is during the summer. Increasing of the kinetic energy during the fall indicates the transition of the circulation to the winter regime. The results are in agreement with analysis of altimetric data by Korotaev & Khomenko (2003), Korotaev et al. (2001) and computations of Staneva & Stanev (1998).

Table 5. Results of calculating mean velocities and the kinetic energy.

Month	**Kinetic Energy** cm^2/s^2
January	95.97
February	89.84
March	76.75
March	50.84
April	88.2
May	33.5
May	44.05
June	20.51
June	35.17
July	33.8
August	43.28
September	105.57
October	68.23
October	52.83
October	56.67
November	76.87
November	130.82
November	99.36

The amount of the available data is not sufficient to monitor detailed monthly variability of the Black Sea surface circulation however is quite complete to give the conclusions about a general tendency of seasonal changes in the water movement.

CHAPTER 3.

Laboratory modeling of the baroclinic instability and transient features of mesoscale surface of the Black Sea

3.1. Introductory Remarks

In this chapter, the laboratory set-up, visualization and measuring techniques that we employ in our experiments are described in section 3.2, while section 3.3 contains the results and analysis of the experiments. Section 3.3 also includes an analysis of the main control parameters of the flow and the dynamical similarity between the laboratory flows and the flows in the Black Sea. We conclude with a discussion of our results in section 3.4. This chapter is mainly based on the recent paper by Blokhina & Afanasyev (2003).

In the new series of experiments reported herein, we follow in general the approach proposed in Bulgakov et al. (1996 b) and Zatsepin et al. (2002) which includes forcing the circulation by a buoyancy source. The present study is focused on the modeling of the unstable peripheral boundary current within a scaled model of the Black Sea. We will show that the laboratory model correctly reproduces the main features of the circulation system including meanders and mesoscale eddies occurring due to the finite amplitude development of the baroclinic instability of the boundary current.

Seasonal variations of river inflow or wind stress cause variations of the intensity of the circulation. We reproduce these transient effects by varying the rotation rate of the platform in the second series of our experiments. The slow-down of the background rotation corresponds to the intensification of the cyclonic circulation in the laboratory basin while the spin-up of the platform models the attenuation of the circulation. The results of these experiments demonstrate the occurrence of the transient features typical of the circulation in the Black Sea. We believe that specific features of the geometry of the coastline are important for the formation of some distinct features of the circulation, namely the big hook-shaped meanders, Batumi and Sevastopol eddies. The laboratory experiments described in this paper demonstrate in particular that the Batumi and Sevastopol eddies are transient features which occur due to the separation of the boundary layer in the eastern part of the sea and at the tip of the Crimean peninsula. Complete dynamical similarity of laboratory flows and the flows in the Black Sea was satisfied in our experiments with respect to the normalized Rossby deformation radius, the Rossby number and the Ekman number.

3.2. Laboratory apparatus and technique

Our experiments were carried out in a rectangular Plexiglas tank of dimensions 64×64-cm, mounted on a rotating table to reproduce the effects of the Earth's rotation (Figure 18). A 2D scale model (15.2 km in 1 cm) of the Black Sea made from Styrofoam was placed into the tank along the diagonal. The shape of the model reproduces the shape of the 50 m isobar (Figure 1). The maximum longitudinal dimension of the model was 75.5 cm. The tank was rotated about a vertical axis through its center in the counterclockwise direction. The rotation rate Ω was varied between 1.55 s^{-1} and 3.1 s^{-1} (period T = 2 - 4 s). The tank itself was filled with salt water of salinity S = 15.00 $^0/_{00}$ -18.75 $^0/_{00}$ (density ρ = 1012 - 1015 kg/m^3) with a working depth of 7 cm. Fresh water was supplied through a thin glass tube from a Mariotte siphon, which allowed us to maintain a constant flux. A typical value of flux in our experiments was 4.5 g/s. The wedge-shaped nozzle filled with a porous material was fixed at the end of the glass tube to reduce the turbulence generated by the fluid inflow. The wedge was submerged just below the surface of the salt water in the "western" part of the sea. The fresh water, flowing horizontally in the cyclonic direction, gradually forms a very thin wedge-formed layer along the periphery of the sea.

The freshwater current was made visible by dying the fluid with the pH-indicator thymol blue. The thymol blue technique (e.g. Baker, 1966, Voropaev and Afanasyev, 1994) utilizes the color change of thymol blue indicator molecules in the presence of a local concentration of base ions. In its neutral state, the solution of thymol-blue is orange-yellow in color. By adding a small quantity of base solution, the fluid turns a dark blue color permitting a visualization of the flow and providing a good contrast for photography. After each experiment, it took only a few minutes for the diffusive chemical reaction with the acidic ambient fluid (an acid was added to the fluid in the tank) to restore the working fluid to its original yellow color. The fluid was illuminated by a diffuse light source from below. A video camera was mounted above the tank on the turntable so that video recordings were obtained in the rotating frame. The camera provides a frame rate of 30 fps and resolution 720×576 pixels.

The horizontal velocity and vorticity fields in the flow were measured using a PIV technique. Small plastic pellets of a mean size of approximately 2×2 mm were seeded on the surface of the fluid to provide flow tracers for the PIV in addition to color contrast.

3.3. Experimental results and interpretation

In what follows we will focus successively upon the evolution of the baroclinic instability in the laboratory basin as well as upon the transient processes involved in the eddy formation during spin-up or slow-down of the circulation.

3.3.1. Baroclinic instability

A series of experiments was performed for different values of the rotation rate of the platform (Figure 18). In all of the experiments, the development of the meanders, which are typical of baroclinic instability, was observed. The wavelengths changed according to equation (1 - 2) and finally were selected to keep the best geometrical similarity between the experiment and the real sea.

Almost immediately after the source of fresh dyed water starts, the narrow boundary current forms and propagates in a cyclonic direction following the coastline (Figures 20 - 21). The current becomes unstable and forms meanders which grow and separate from the current forming mesoscale eddies. Interesting events of pairing of eddies can be observed during the finite amplitude stage of evolution of the instability (Figure 21). These events increase the wavelength of the instability twofold. However, after the eddies separate, the instability of the boundary current develops again with the same typical wavelength. The development of instability can be observed both along the "southern" shore and "northern" shore of the sea. Separated eddies eventually fill the interior of the basin forming a typical pattern of a quasi-two-dimensional turbulent flow.

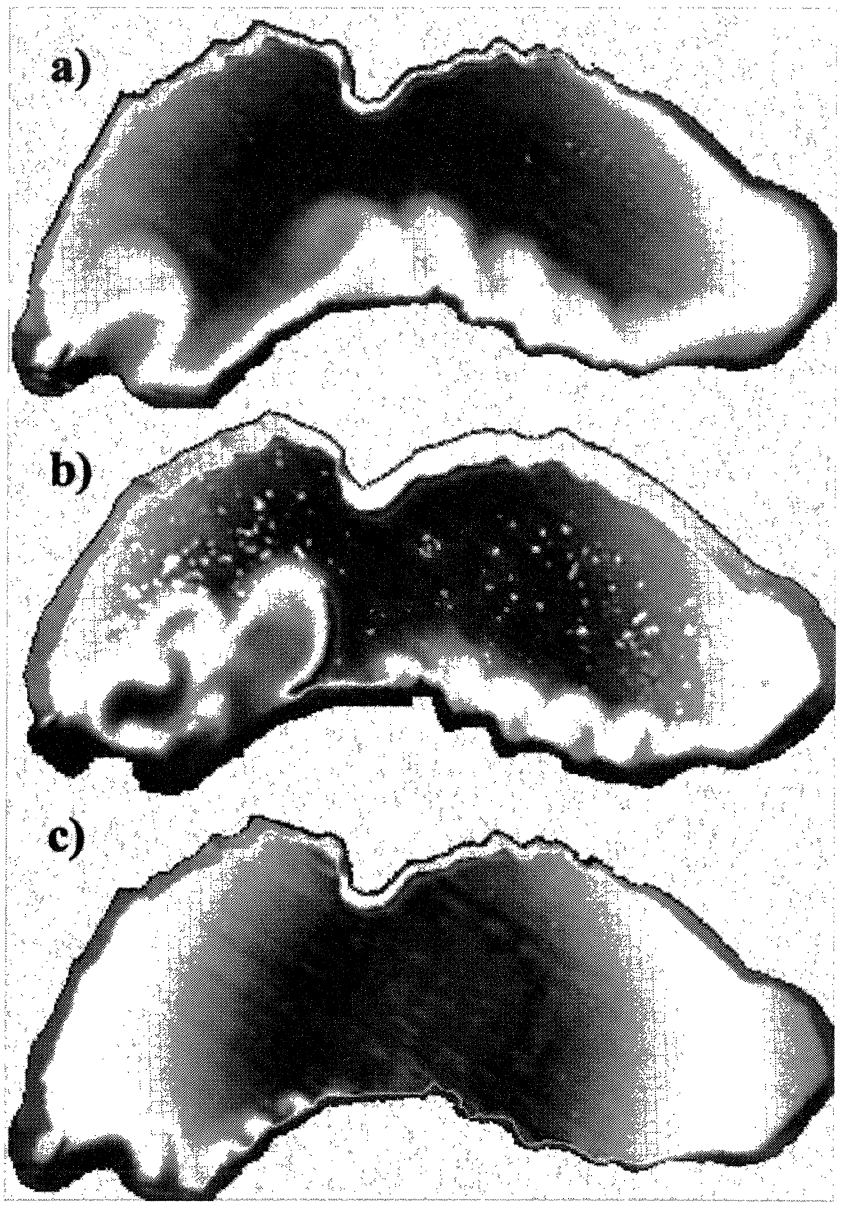

Figure 19. Dependence of the baroclinic wavelength on the speed of platform rotation. Rotation rate $\Omega = 1.57\ s^{-1}$ (T = 4s) **(a)**, $2.33\ s^{-1}$ (T = 2.7 s) **(b)**, $3.14\ s^{-1}$ (T=2s) **(c)**; wavelength λ = 6.32 **(a)**, 4.41 **(b)**, 2.6 cm **(c)**.

Striking similarities between the laboratory flow and the real flow in the Black Sea can be observed in particular in the region of the flow which corresponds to the southern coast between 30 and 33°E. A regular array of relatively small scale meanders (Figures 20 -

21) is often observed in satellite imagery (Figure 3). The development of large hook-shaped meanders was also documented in this region (e.g. meander M6 in Figure 8 in Oguz, Besiktepe, 1999). Since cyclonic vorticity is located at the left-hand side of the meander while anticyclonic vorticity is located at the right-hand side, these meanders can also be interpreted as mushroom-formed currents (e.g. sketch in Figure 1 in Ginzburg et al., 2000). The laboratory flow forms very similar features (Figure 21c) which gives an indication that some particular features (most likely the curvature) of the coastline are important for the formation of these flows.

Considering the experiments in the sequence from small to larger rotation rates it will be observed that the wavelength of the instability decreases (Figure 20). The results of measurements of the wavelength for different values of rotation rate and accordingly R_d are shown in Figure 22. To estimate R_d the values of the thickness h of the upper layer is required. These values were estimated from the experimental images of the flows by measuring the surface area of the boundary current for different times. Since the value of the flux rate q is known one can easily estimate the vertical extent of the fresh layer by dividing the total volume of the layer for given time by its surface area. The mean value $h = 2.0 \pm 0.2$ cm was obtained in our experiments. Linear regression then gives the value of the proportionality factor between the length of baroclinic waves and Rossby radius of deformation to be equal 4.3 ± 0.4 which is in close agreement with theory.

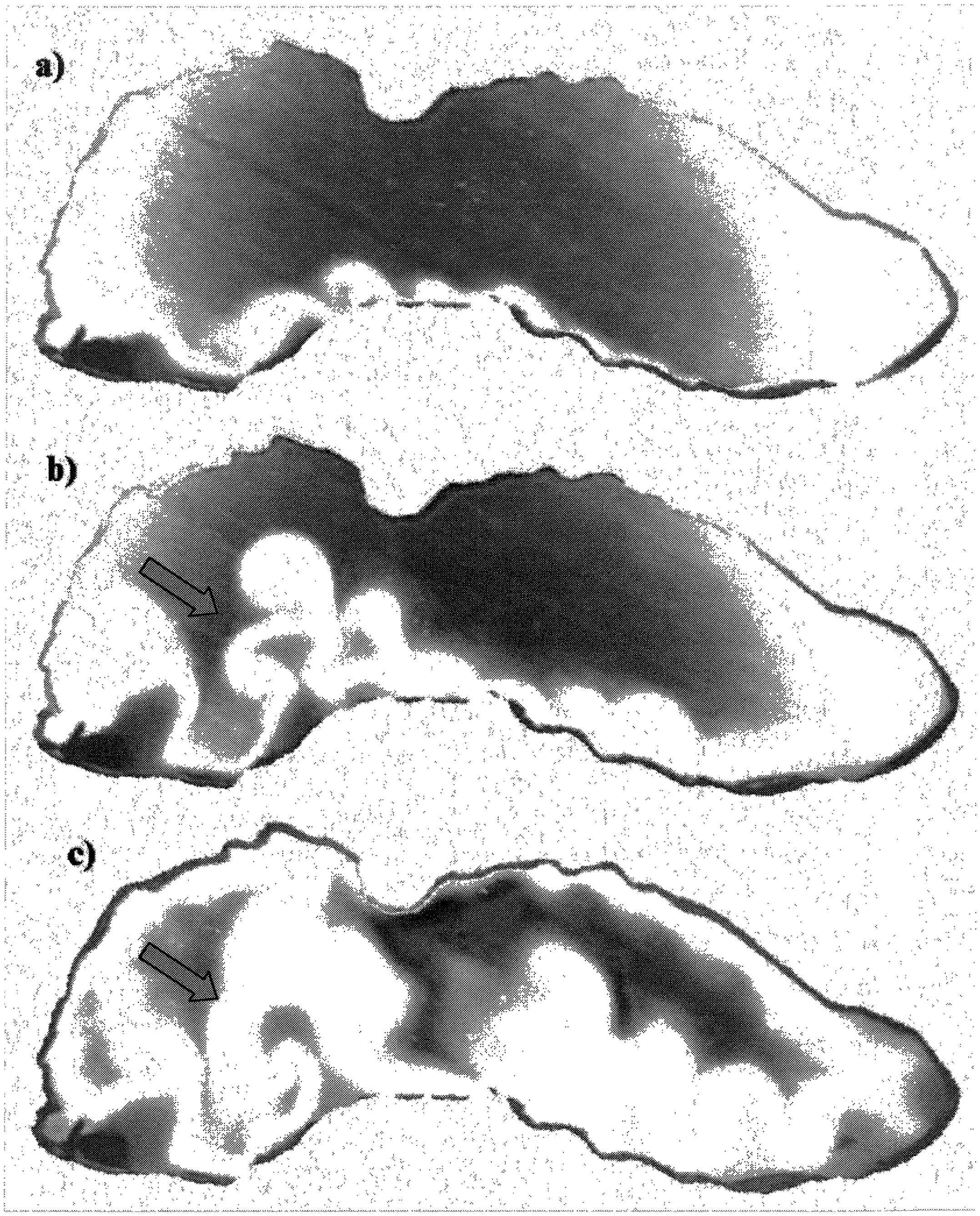

Figure 20. Sequence of video frames that shows the typical evolution of the boundary current and baroclinic instability: $t = 9$ (a), 72 (b), 274 s (c). Visualization is by thymol blue. Rotation rate $\Omega = 2.1\ s^{-1}$. The arrows indicate the process of pairing of eddies (b) and the formation of a big hook-shaped meander (c).

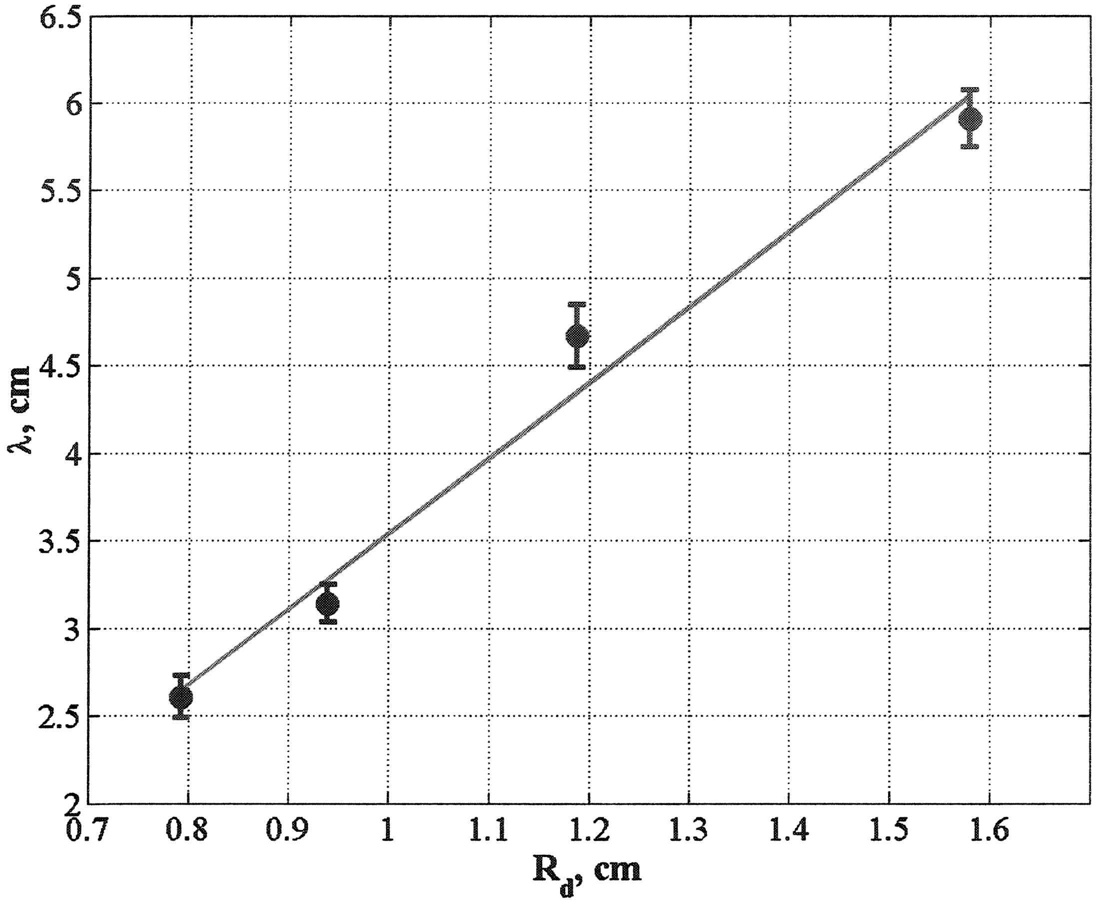

Figure 21. Variation of the wavelength of baroclinic waves with the Rossby radius of deformation. Solid line is the result of linear regression.

3.3.2. Control parameters

An important issue that allows us to make the quantitative comparison of the major characteristics of our laboratory flows with that in the Black Sea is the dynamical similarity. We have achieved similarity with respect to a number of control parameters. The natural scale of the baroclinic motions is represented by the Rossby radius of deformation. Taking the thickness of the boundary current h = 100 - 200 m [e.g. Oguz & Besiktepe (1999)] and the salinity difference $\Delta S = 3^0/_{00}$, one can obtain the value of the Rossby radius for the Black Sea to be R_d = 15-20 km. The Rossby radius, normalized by the scale of the sea L = 300 km, gives the dimensionless parameter R_d/L = 0.05 – 0.07 which characterizes the relative size of baroclinic motions with respect to the size of the basin. One can also interpret this parameter as a ratio of the distance covered by long baroclinic waves per one rotation of the system to the size of the basin. The appropriate value of the length scale for the laboratory basin is L = 20 cm while the Rossby radius varies between 0.8 and 1.6 cm. This gives R_d/L = 0.04 – 0.08 for the laboratory flows. Thus, there is similarity between the normalized wavelength of the instability of the scale of mesoscale vortices in the laboratory and in the Black Sea. Since the laboratory basin is a scale model of the sea, the size of the eddies with respect to the typical size of the coastal features is also similar. Direct measurements of the wavelength of the instability in the Black Sea using satellite imagery (e.g. Figure 3) gives λ = 70 – 80 km. Comparing these values with the estimates for the Rossby radius of deformation, one obtains c = 4 – 4.5 which is in agreement with the results of our experiments. It is interesting to note that the normalized width of the boundary current W/L was also similar to that in the Black Sea. In the laboratory W = 2.5 – 5 cm that gives W/L = 0.13 – 0.25. In the Black Sea the width of the Rim Current can be estimated to be W = 40 –80 km which gives the similar range of W/L = 0.13 – 0.27. This fact, however, is just another consequence of the similarity of the Rossby radius of deformation.

The Rossby number, which is defined as

$$Ro = \frac{U}{fL},$$

where U is a typical velocity, gives the ratio of the vorticity of the flow to the background vorticity. Taking the typical values of the velocity in the Rim Current jet to be U = 30 – 80 cm/s, we obtain Ro = 0.01 – 0.02 for the basin-size circulation. The speed of the boundary current for the laboratory flow was measured in the experiments with seeding particles. The speed varies between U = 2 cm/s in the vicinity of the source along the "southern" shore and U = 1 cm/s along the "northern" shore. Accordingly the value of the Rossby number varies in the range Ro = 0.01 – 0.03. The similarity of the values of the Rossby number in the laboratory and in the Black Sea can also be interpreted in terms of the normalized time T which gives the number of days required for the current to complete a full circle around the sea. This time scale is proportional to $1/Ro$. The estimates give T = 60 – 90 days for both the laboratory and the Black Sea. It is also useful to introduce the local Rossby number $Ro_l = \frac{U}{fl}$, where l is the size of the mesoscale eddies. For the laboratory flows, l = 4 – 10 cm which gives Ro_l = 0.04 – 0.12. Similar values of Ro_l were obtained for the mesoscale eddies in the Black Sea from the direct calculation of the velocity field of the surface circulation using the satellite data [Afanasyev et al. (2002)]. Thus the values of the Rossby number are identical for the laboratory flows and the flows in the Black Sea. Therefore the dynamical regime of vortices is similar. In particular the fact that the Rossby number is small indicates that the vortices are to a large extent in geostrophic balance.

A further important dimensionless parameter is the Ekman number

$$Ek = \frac{\nu_z}{fh^2},$$

where ν_z is the vertical viscosity. This parameter characterizes the damping of eddies due to Ekman pumping. The vorticity in the eddy will decay exponentially with the characteristic time scale

$$T_E = \frac{2}{fEk^{1/2}} \ .$$

It is difficult to estimate the Ekman number for the flows in the sea because the vertical viscosity is unknown. Using the value $\nu_z = 1$ cm^2/s [Zatsepin et al. (2002)] we obtain $Ek = 10^{-4}$. In the laboratory flow, the vertical exchange of momentum is provided by molecular viscosity which gives the value of the Ekman number $Ek \approx 6\times10^{-4}$. The damping rate is therefore slightly higher for the laboratory flows. The time scale T_E is then approximately equal to 20 s or 5 laboratory "days".

3.3.3. Transient flows

The second series of experiments we performed were directed at the investigation of transient effects occurring when the circulation in the Black Sea varies due to seasonal changes of the river input or the atmospheric forcing. Suppose the cyclonic wind forcing becomes stronger over a period of say one month. This will cause the appropriate change in the vorticity of the interior of the basin. Strictly speaking the total vertical vorticity is always zero because of the no-slip conditions at the boundaries. The cyclonic circulation in the major part of the basin therefore becomes more intense. The vorticity (velocity shear) in the relatively narrow anticyclonic boundary layer also becomes stronger. The increase of the anticyclonic wind forcing on the other hand will cause the opposite effect – the attenuation of the cyclonic circulation. It is difficult to model the wind forcing in the laboratory because such a forcing cannot be easily controlled and measured. Another way to model the relative changes of the circulation in the basin is to vary the rotation rate of the platform. The slow-down of the platform will correspond then to the intensification of the cyclonic circulation while the spin-up of the platform will model the attenuation of the circulation. It is straightforward then to describe the initial motion of water in the basin using simple theory. When the boundaries of the basin start rotating with respect to the water at rest the water does not follow the rotation of the basin but it only undergoes an irrotational displacement with respect to the boundaries of the basin. The real flows are subject to no-slip boundary conditions which result in formation of the boundary layer with vorticity of the opposite sign. The dynamics of the boundary layer will produce interesting effects, in particular the separation of the boundary layer. We believe that the process of the separation of the boundary layer is responsible for the formation of the Batumi and Sevastopol eddies in the Black Sea as well as for the effect of the reversal of the circulation in the region of the Batumi eddy. These processes can be illustrated in the simple experiments (Figures 22 - 23). Figure 22 demonstrates the flows resulting from the slow-down of the platform from Ω=1.8 to 1.55 s^{-1} during 10 laboratory "days". The slow-down was performed when the boundary current was established all around the coastline. These conditions therefore correspond to the intensification of the circulation in the entire basin when the peripheral jet current is well-formed. Further development of the flow is characterized by the formation of two typical features. The first one is the separation of the boundary current from the "northern" shore in the "eastern" part of the sea. The recirculation in the extreme eastern part of the sea is cyclonic which is opposite to that of the Batumi eddy. We believe that this circulation pattern corresponds to the fall circulation in the Black Sea according to the geostrophic velocity maps deduced from the TOPEX/Poseidon altimeter data [see Figure 9 d in Korotaev et al. (2001), Figure 6 f in Korotaev et al. (2003)]. It is interesting that in the same picture in Korotaev et al. (2001) the Sevastopol eddy is most intense compared to other seasons. The anticyclonic eddy can be also observed in the region where the boundary current separates from the tip of the Crimean peninsula in the laboratory flow. Figure 23 demonstrates a typical pattern of the circulation occurring in a similar experiment with the slow down of the platform. In contrast to the previous experiment, however, the boundary current was initially very weak (the source was switched off). In this case the separation occurs from the "southern" shore and the resulting recirculation corresponds to that in the Batumi eddy [see Figure 9 b in Korotaev et al. (2001)]. Thus, there are obvious similarities between certain features of the circulation in the Black Sea and in the laboratory caused by the separation of the boundary current. These features are transient in a sense that they occur due to the variation of the global circulation in the basin.

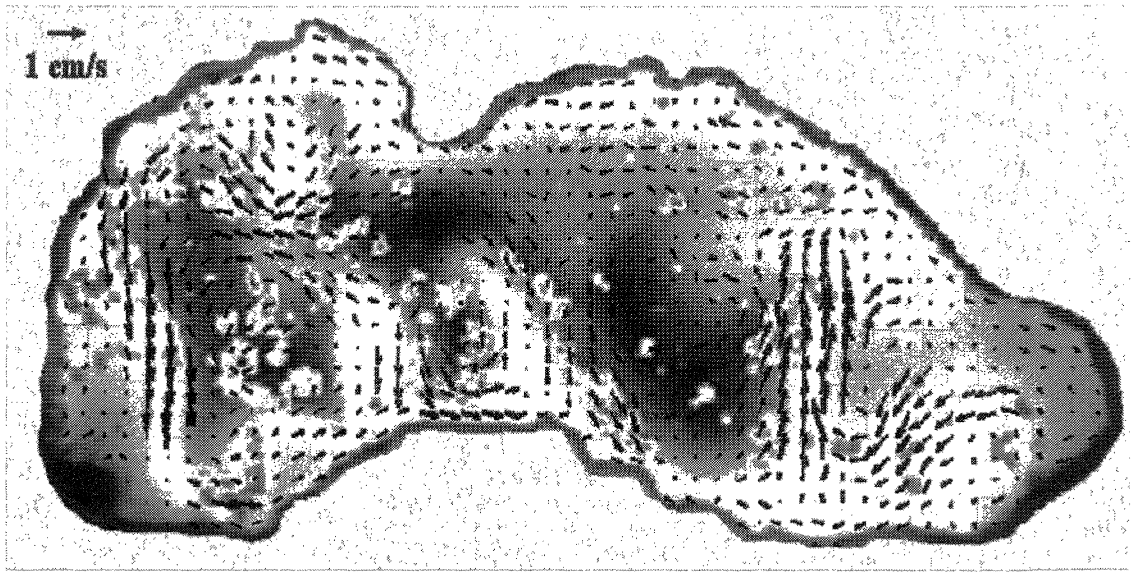

Figure 22. Experimental image of the flow with tracer particles during the slow-down of the rotating platform. Rotation rate is decreased from $\Omega = 1.8$ to $1.6\ s^{-1}$ during 10 revolutions of the platform. Velocity field (arrows) is obtained by PIV method.

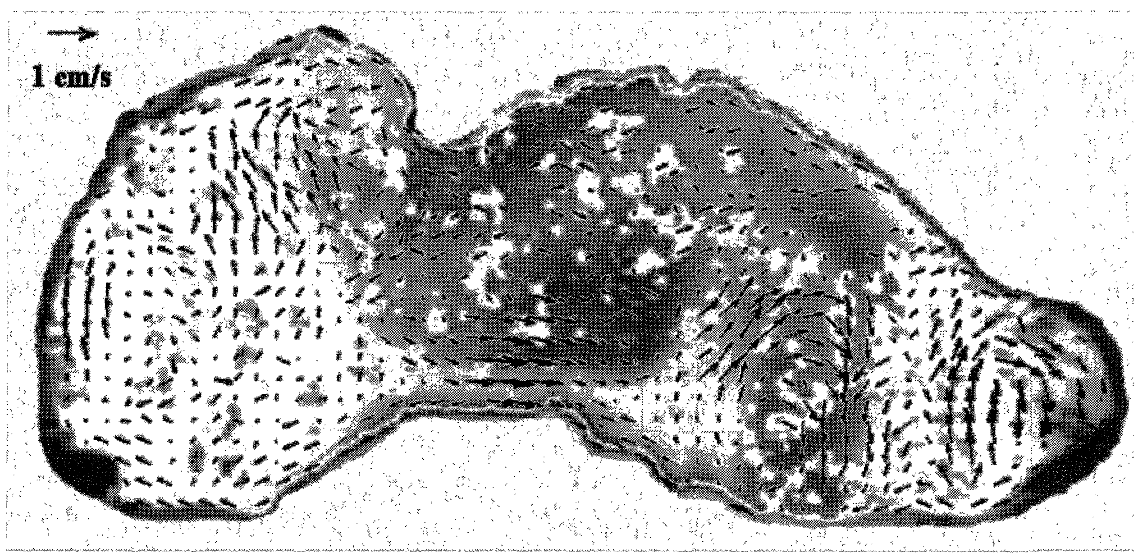

Figure 23. The same as in Figure 22 but when the source of fresh water was switched off before the slow-down of the platform.

3.4. Conclusions

The laboratory experiments described herein provide clear evidence that baroclinic instability is an important dynamical feature of the circulation in the Black Sea. The results demonstrate the occurrence of the cyclonic peripheral jet current, which develops according to the general theory described by the thermal wind equations. This main current system then becomes unstable and forms typical meanders and mesoscale eddies which eventually fill the interior of the basin forming a typical pattern of quasi-two-dimensional turbulent flow. It is interesting to consider a mechanism of intensification or attenuation of the global circulation in the Black Sea. It is known that variations in the intensity of the circulation occur due to variations of the fresh water input by rivers and the variation of wind forcing. The transfer of vertical vorticity to the interior of the basin occurs differently in these two cases. When the intensity of the boundary current varies, the interior of the basin is not immediately affected. The perturbation to the circulation is localized in the narrow peripheral region of the width of the order of the Rossby radius of deformation. Baroclinic instability, however, provides an effective mechanism of transfer of cyclonic vorticity into the interior of the basin. Cyclonic eddies form at the left-hand side of the unstable boundary current while anticyclonic eddies form at the right-hand side near the boundary. The cyclonic eddies then grow and penetrate the interior contributing to its overall cyclonic circulation. Anticyclonic vorticity on the other hand remains at the boundary and forms the boundary layer. We believe that the formation of the anticyclonic boundary layer is due to baroclinic instability rather than to the no-slip boundary condition and horizontal transfer of vorticity by viscosity. The coefficient of the turbulent horizontal exchange of momentum however can be introduced here to account for this effect. This is widely used in numerical models that are often too coarse to resolve the small-scale instability. In contrast to this indirect transfer of vorticity by cyclonic eddies, the wind forcing transfers vorticity directly to the entire basin. To simulate this effect to some extent we varied the rotation rate of the platform, thus varying the relative vorticity of the fluid. Although there are certain similarities between the transient eddies in the Black Sea and in the laboratory flows, the mechanism of generation of anticyclonic vorticity in the boundary layer due to the no-slip lateral boundary condition and the transfer of vorticity by molecular viscosity can be important for the laboratory flows. Thus, it is difficult to provide any quantitative comparison between the resulting separation of the boundary layer in our experiments where the rotation rate was varied and the separation of the Rim current in the Black Sea. Further experiments that can clarify this mechanism are clearly required and are currently under way.

Bibliography

Afanasyev Y.D., A.G. Kostianoy and A.G. Zatsepin, 2002, Analysis of Velocity Field in the Eastern Black Sea from satellite data during the «Black Sea'99» Experiment, *J. Geophys. Res. – Oceans*, 107 (C8) 10.

Baker, D.T., 1966, A technique for the precise measurements of small fluid velocities, *J. Fluid Mech.*, 26, 573.

Beckers J. M., M. Gregoire, J. C. J. Nihoul, E. Stanev, J. Staneva and C. Lancelot, 2002, Modelling the Danube-influenced North-western Continental Shelf of the Black Sea. I: Hydrodynamical Processes Simulated by 3-D and Box Models, *Estuarine, Coastal and Shelf Science,* 54, 453–472.

Blokhina M. D., Y. D. Afanasyev, 2003, Baroclinic instability and transient features of mesoscale surface circulation in the Black Sea: Laboratory experiment, *J. Geophys. Res.*, 108(C10), 3322.

Bogatko, O. N., S. G. Boguslavsky, Y. M. Beliakov, and R. E. Ivanov, 1979, Surface currents in the Black Sea (in Russian), in *Kompleksnye Issledovaniya Chernogo Morya*, pp. 25– 33, Mar. Hydrophys. Inst., Sevastopol, Ukraine.

Bulgakov S. N., G. K. Korotaev, and J. A. Whitehead, 1996a, The Role of Buoyancy Fluxes in the Formation of a Large-Scale Circulation and Stratification of Sea Water: 1. Theory, *Izvestiya, Atmospheric and Oceanic Physics*, 32, No. 4, p. 506-513.

Bulgakov S. N., G. K. Korotaev, and J. A. Whitehead, 1996b, The Role of Buoyancy Fluxes in the Formation of a Large-Scale Circulation and Stratification of Sea Water: 2. Laboratory Experiments, *Izvestiya, Atmospheric and Oceanic Physics*, 32, No. 4, pp. 514-520.

Charney, J. G., 1947, The dynamics of long waves in a baroclinic westerly current. *J. Meteor.*, 4, pp. 135-163.

Cushman - Roisin B., 1994, *Introduction to geophysical fluid dynamics*, Englewood Cliffs, N.J., Prentice Hall, 320 p.

Demyshev,S. G., V. V. Knysh, G. K. Korotaev, O. A. Saenko, and V. Chernov, 1996, A comparative estimation of the accuracy of reconstruction of the Black Sea hydrophysical parameters through assimilation of in situ and satellite observations into a model: numerical experiments. *Oceanology* , **36**, No. 5, pp. 671-680

Eady, E., 1949, Long waves and cyclone waves, *Tellus*, 1, pp. 33-52.

Efimov V. V., M. V. Shokurov, and V. S. Barabanov, 2002, Physical Mechanisms of Wind Circulation Forcing over the Inland Seas, *Izvestiya, Atmospheric and Oceanic Physics*, 38, No. 2, pp. 247-258.

Efimov V. V., M. V. Shokurov, 2002, Spatiotemporal Structure of the Surface Wind Field over the Black Sea *Izvestiya, Atmospheric and Oceanic Physics* , 38, No. 4, pp. 421.

Emery, W., C. Fowler, and J. Maslanik, 1995, Satellite remote sensing of ice motion, in *Oceanographic Applications of Remote Sensing*, ed. Motoyoshi Ikeda and Frederic W. Dobson. CRC Press, Boca Raton.

Eremeev V.N.(ed.), 1992, *Complex Oceanographic Research on the Black Sea*, 130 pp., VSP, The Netherlands.

European Environment Agency, "The rivers of the Black Sea", 2002, Technical report No 71, prep. by Shalva Jaoshvili, 58 pp.

Falkner, K. Kenison, D.J. O'Neill, J.F. Todd, W.S. Moore and J.M. Edmond, 1991, Depletion of barium and radium-226 in Black Sea surface waters over the past thirty years, Nature, v. 350, pp. 491-494.

Fedorov, K. N., A. I. Ginzburg, 1992, Mushroom-shaped currents (eddy dipoles): One of the most common forms of coherent movement in the ocean in *Coherent Structures and Self-Organisation of Oceanic Motions*, pp. 12– 20, Nauka, Moscow, (in Russian).

Filippov, D.M., 1968, Circulation and structure of the Black Sea waters, 136 pp, Nauka, Moscow, (In Russian).

Fincham, A. M., and G. R. Spedding, 1997, Low cost. high resolution DPIV for measurement of turbulent fluid flow, *Exp. Fluids*, 23, pp. 449– 462.

Fjørtoft, R., 1950, Application of integral theorems in deriving criteria of stability for laminar flows and for the baroclinic circular vortex. *Geofys. Publ.*, 17, No 6, pp 1-52.

Gill, A. E., 1982, *Atmosphere-Ocean Dynamics*. Academic Press, New York, 662 p.

Ginzburg A. I., A. G. Kostianoy, V. G. Krivosheya, N. P. Nezlin, D. M. Soloviev, S. V. Stanichny, and V. G. Yakubenko, 2002a, Mesoscale eddies and related processes in the northeastern Black Sea, *Journal of Marine Systems*, 32 (1-3), pp. 71–90.

Ginzburg A. I., A. G. Kostianoy, N. P. Nezlin, D. M. Soloviev, and S. V. Stanichny, 2002b, Anticyclonic eddies in the northwestern Black Sea, *Journal of Marine Systems*, 32 (1-3), pp. 91–106.

Ginzburg, A. I., A.G. Kostianoy, D. M. Soloviev, and S. V. Stanichny, 2000, Remotely sensed coastal/deep – basin water exchange processes in the Black Sea surface layer, in

Satellites, Oceanography and Society, edited by D. Halpern, pp. 273-287, Elsevier, Amsterdam.

Ginzburg, A. I., E. A. Kontar, A. G. Kostianoy, V. G. Krivosheya, S. V. Stanichny, S. Y. Laptev, and D. M. Soloviev, 1998, System of synoptic eddies over continental slope of the north-western Black Sea in summer 1993 (satellite and CTD data), Okeanology, 38, pp. 56–63.

Ginzburg, A. I., 1994, Horizontal exchange processes in the near-surface layer of the Black Sea (in Russian), *Issled. Zemli Kosmos.*, 2, pp. 75– 83.

Ginzburg, A. I., 1995, On nonstationary jet-like currents in the southwestern Black Sea (in Russian), *Issled. Zemli Kosmos.*, 4, pp. 10– 16.

Knysh V.V., Demyshev S.G., Korotaev G.K., Sarkisyan A.S. 2001, Four - dimensional climate of seasonal Black Sea circulation // Russ. J. Num. Anal. Math. Modelling. V. 16, n. 5. pp. 409-426.

Korotaev G. K., Khomenko G. A., 2003, Lagrangian Transport by Currents Variable in Time in the Model of Wind-Induced Circulation of the Black Sea, Physical Oceanography, V. 13 (2), p.75-87

Korotaev, G. K., O. A. Saenko, and C. J. Koblinsky, Satellite altimetry observations of the Black Sea level, *J. Geophys. Res.*, 106, C1 , 917-934, 2001.

Korotaev, G.K., T. Oguz, A. M. Nikiforov, C. J. Koblinsky, 2003, Seasonal, interannual, and mesoscale variability of the Black Sea upper layer circulation derived from altimeter data, *J. Geophys. Res.*, 108, C4, 3122.

Kourafalou V. H. and E. V. Stanev, 2001, Modeling the impact of atmospheric and terrestrial inputs, on the Black Sea coastal dynamics, *Annales Geophysicae*, 19, pp. 245–256.

Kundu P. K., 1990, *Fluid Dynamics,* San Diego, Academic Press, 638 p.

Kuo, H. L., 1949, Dynamic instability of two-dimensional nondivergent flow in a barotropic atmosphere. *J. Meteor.*, 6, pp. 165-185.

Maderich V., S. Konstantinov, 2002, Seasonal Dynamics of the System Sea-Strait: Black Sea-Bosphorus Case Study, Estuarine, Coastal and Shelf Science, Vol. 55, No. 2, pp. 183-196

Mysak, L. A., and F. Schott, 1977, Evidence of baroclinic instability in the Norwegian Current, J. Geophys. Res., 82, pp. 2087–2095.

Mysak, L. A., E.R. Jonhson, W. W. Hsieh, 1981, Baroclinic and barotropic instabilities of coastal currents. J. Phys. Oceanogr., V. 11, p. 209-23. 43

Neumann, G., Die absolute topografie des physikalischen Meeresniveaus und die Oberflachen-stromungen des Schwarzen Meeres, *Ann. Hydrogr. Mar. Meteorol.*, 70, 265–282, 1942.

Oguz, T. and P. Malanotte-Rizzoli, Seasonal variability of wind and thermohaline driven circulation in the Black Sea: Modeling studies, *J. Geophys. Res.*, 101, 16551-16569, 1996.

Oguz, T. and S. Besiktepe, Observations on the Rim Current structure, CIW formation and transport in the Western Black Sea, *Deep Sea Research*, I, 46, 1733-1753, 1999.

Oguz, T., P. E. La Violette, and U. Unluata, The Upper layer circulation of the southern Black Sea: Its variability as inferred from hydrographic and satellite observations, *J. Geophys. Res.*, 97, C8, 12569-12584, 1992.

Oguz, T., V. S. Latun, M. A. Latif, V. V. Vladimirov, H. I. Sur, A. A. Markov, E. Ozsoy, B. B. Kotovshchikov, V. V. Eremeev, and U. Unluata, Circulation in the surface and intermediate layers of the Black Sea, *Deep Sea Research*, 40 (8), p.1597-1612, 1993.

Ozsoy E. and Unluata U., Oceanography of the Black Sea: a Review of Some Recent Results, 1997, Earth Sci. Rev., 42, (4), 231-272.

Panteleev G. G., N. A. Maximenko, B. deYoung, C. S. Reiss, and T. Yamagata, 2002, Variational interpolation of circulation with nonlinear, advective smoothing, *J. Atmos. Oceanic Tech.* 19:1442-1450.

Pawlak, G., and L. Armi, 1998, Vortex dynamics in a spatially accelerating shear layer, *J. Fluid Mech.*, 376, 1– 35.

Pedlosky, J., 1987, *Geophysical Fluid Dynamics,* Springer-Verlag, New York, 2 edition, 710p.

Phillips, N. A., 1951, A simple three-dimensional model for the study of large-scale extratropical flow patterns. *J. Meteor.*, 8, pp. 381-394.

Pierrehumbert R. T., K.L. Swanson, 1995, Baroclinic Instability, Ann.Rev. Fluid Mech., V.27, p. 419 - 67

Rayleigh, Lord, 1880, On the stability, or instability, of certain fluid motions. *Proc. London Math. Soc.*, 9, pp. 57-70.

Smith, P. C., 1976: Baroclinic instability in the Denmark Strait over-flow. *J. Phys. Oceanogr.,* **6,** 355–371.

Stanev, 1990, On the mechanisms of the Black Sea circulation, Earth - Science Reviews, V. 28, pp. 285-319.

Stanev, E. V., and J. M. Beckers, Barotropic and baroclinic oscillations in strongly stratified ocean basins. Numerical study for the Black Sea. *J. Mar. Sys*., 19, 65-112, 1999.

Stanev, E. V., and J. V. Staneva, The impact of the baroclinic eddies and basin oscillations on the transitions between different quasi-stable states of the Black Sea circulation, *J. Mar. Sys.,* 24,1-2,3-26, 2000.

Staneva, J.V., Dietrich, D.E., Stanev E.V., Bowman, M.J., Rim current and coastal eddy mechanisms in an eddy-resolving Black Sea general circulation model, *J. Mar. Sys.*, 31, 137-157, 2001.

Sutcliffe, R. C. 1951, Mean upper contour patterns of the Northern Hemisphere - the thermal-synoptic view pattern. *Quart. J. Roy. Meteor. Soc.* 77, pp. 435-440

Titov, V. B., Characteristics of the main Black Sea current and near-shore anticyclonic eddies in the Russian sector of the Black Sea, *Oceanology*, 42 (5), 637-645, 2002.

Unluata, U., T. Oguz, M.A. Latif, E. Ozsoy, On the physical oceanography of the Turkish Straits, In *The Physical Oceanography of the Sea Straits*, L.J. Pratt (Ed.). NATO/ASI Series, V.318, p.25-60, Kluwer Academic Publishers, Dordrecht, 1990.

Verdiere de C., T Huck, Baroclinic instability: an oceanic wavemaker for interdecadal variability, 1999, *Journal of Physical Oceanography*, **29**, 893-910.

Voropayev, S. I., and Y. D. Afanasyev, *Vortex Structures in a Stratified Fluid*, 230 pp., Chapman and Hall, New York, 1994.

Wright, D.G., 1987, Baroclinic Instability: Energy Transfer and the Role of Potential Vorticity Conservation, *Atmosphere - Ocean*, V. 25 (3), pp. 225 - 241

Wright, D.G. 1981, Baroclinic Instability in Drake Passage, *J. Phys. Oceanography*, V. 11, pp. 231 - 246

Zatsepin A. G., A. I. Ginzburg, A. G. Kostyanoy, V. V. Kremenetskiy, V. G. Krivosheya, S. G. Poyarkov, Yu. B. Ratner, A. Yu. Skirta, D. M. Soloviev, S. V. Stanichny, O. Yu. Stroganov, N. A. Sheremet, and V. G. Yakubenko, Variability of Water Dynamics in the Northeastern Black Sea and Its Effect on the Water Exchange between the Near-Shore Zone and Open Basin, *Oceanology*, 42, Suppl. 1, pp. S1-S15, 2002

Appendix 1.

Table 6. The list of all available pairs of satellite images

N	Month	Year	Images, tif	Time between images	Time, min
1	January	2002	247-24W	1 h 50	110
2	January	2002	247-257	25 h 40 min	1540
3	January	2002	25E-256	1 h 50	110
4	February	2000	122-125	2 h 45 min	165
5	March	2000	242-245	3h 45 min	225
6	March	2000	242-243	1 h 55 min	115
7	March	2000	243-245	1h 50 min	110
8	April	2002	286-281	2h 30min	150
9	May	2000	204-202	8 h 00 min	480
10	May	2000	204-205	11h 20 min	680
11	May	2000	202-205	3 h 20 min	200
12	June	2001	110-111	40 min	40
13	June	2001	110-112	11h 25 min	685
14	June	2001	110-114	3 h 20 min	200
15	June	2001	114-112	8 h 05 min	485
16	June	2001	111-112	10h 45 min	645
17	June	2001	157-155	5h 30 min	330
18	July	2001	147-145	5 h 40 min	340
19	August	2001	286-281	3h 20min	200
20	September	2001	187-180	3 h 30 min	210
21	September	2001	182-185	1h 55 min	115
22	September	2001	184-182	9 h 25 min	565
23	September	2001	186-184	5 h 30min	330

24	October	2001	032-035	55 min	55
25	October	2001	044-042	8 h 55 min	535
26	October	2001	107-105	5 h 50 min	350
27	October	2001	097-095	6 h 05 min	365
28	October	2000	032-033	60 min	60
29	October	2000	033-040	11h 20 min	680
30	October	2000	041-042	10h 25 min	625
31	October	2000	031-032	10h 25 min	625
32	November	2000	166-161	2 h 30 min	150
33	November	2000	161-162	10 h 15 min	615
34	November	2000	160-167	8h 35 min	515
35	November	2000	167-162	2h 55 min	175
36	November	2000	167-163	4 h 00 min	240
37	November	2000	161-167	7h 20 min	440
38	November	2000	166-167	9h50 min	590
39	November	2000	166-162	12h 55 min	775
40	November	2000	162-163	1 h 05 min	65
41	December	1999	021-024	1 h 30 min	90
42	December	1999	021-022	8h 35 min	515
43	December	1999	024-022	7h 05 min	425